THE UNIVERSITY OF CHICAGO

ELECTRONIC CORRELATION IN ORGANOMETALLIC CHEMISTRY: REDUCED DENSITY MATRIX APPROACHES

A DISSERTATION SUBMITTED TO
THE FACULTY OF THE DIVISION OF THE PHYSICAL SCIENCES
IN CANDIDACY FOR THE DEGREE OF
DOCTOR OF PHILOSOPHY

DEPARTMENT OF CHEMISTRY

BY

ANTHONY W. R. SCHLIMGEN

CHICAGO, ILLINOIS

JUNE 2018

To Pat, John, Catherine, and Elizabeth

TABLE OF CONTENTS

LIST OF FIGURES vi

LIST OF TABLES vii

ACKNOWLEDGMENTS viii

ABSTRACT ix

1 INTRODUCTION 1
- 1.1 N-Electron Wavefunction Theory 1
- 1.2 Reduced Density Matrix Formalism 4
- 1.3 Electron Correlation 5
- 1.4 References 6

2 *AB INITIO* QUANTUM CHEMICAL METHODS FOR COMPUTING ELECTRON CORRELATION 11
- 2.1 Introduction 11
- 2.2 Complete Active Space Self Consistent Field Theory 12
- 2.3 Variational 2-RDM Theory 13
- 2.4 Anti-Hermitian Contracted Schrödinger Equation 15
- 2.5 Analytical Gradient Techniques for CASSCF 16
  - 2.5.1 Analytical Gradient of Variational 2-RDM Theory 16
  - 2.5.2 Analytical Gradient for CI Wavefunctions 19
- 2.6 References 20

3 ELECTRONIC STRUCTURE METHODS FOR ORGANOMETALLIC CHEMISTRY 30
- 3.1 Introduction 30
- 3.2 Ligand Field Theory 31
- 3.3 Density Functional Theory and *ab initio* Methods 33
- 3.4 References 34

4 EXAMPLES OF ELECTRON CORRELATION IN ORGANOMETALLIC CHEMISTRY 36
- 4.1 Vanadium oxo 2,6-bis[1,1-bis(2-pyridyl)ethyl]pyridine 36
  - 4.1.1 Introduction 36
  - 4.1.2 Results and Discussion 39
  - 4.1.3 Conclusions 44
  - 4.1.4 References 45
- 4.2 Nickel Dithiolates 51
  - 4.2.1 Introduction 51
  - 4.2.2 Theory and Computational Details 53
  - 4.2.3 Results 54
  - 4.2.4 Conclusions 59

4.2.5 References 61
4.3 Geometry Optimization of CrF_6 and Nickel Dithiolate Revisited 72
4.3.1 Introduction 72
4.3.2 Results 74
4.3.3 Conclusions 80
4.3.4 References 81

LIST OF FIGURES

1.1 Schematic MO's for the dissociation of hydrogen fluoride. 5

3.1 Ligand field splitting for ML_6 with two different field splitting parameters, Δ . . 32

4.1 Structure of vanadium oxo 2,6-bis[1,1-bis(2-pyridyl)ethyl]pyridine. Vanadium is yellow, oxygen red, nitrogen blue, carbon grey, and hydrogen white. 37

4.2 Contour plots of electron density from the (HOMO) natural orbital of the (a) vanadium (IV) oxo and the (b) vanadium (III) oxo complexes are compared. The electron densities are computed at the [42,40] level of theory by the 2-RDM method. In (a) all of the electron density is located on the vanadium oxide moiety in agreement with the ligand-field picture. In (b), however, electron density is spread over not only vanadium oxide moiety but also the π space of the four equatorial pyridine ligands, reflecting the entanglement of the electron among the nearly energetically degenerate pyridine ligands. Generated with contour value 0.03, grid size 1, and 150 grid points. Vanadium is yellow, oxygen is red, nitrogens are blue, carbons are black, and hydrogens are white. 40

4.3 Ligand field theory (LFT) and 2-RDM theory predict different electronic pictures for the reduction of vanadium (IV) oxo (left) to vanadium (III) oxo (right). While the vanadium (IV) oxo complex's electronic structure can be well approximated by the schematic molecular orbital diagram from LFT (left), two different pictures of the vanadium (III) oxo product emerge from the [42,40] 2-RDM and LFT treatments (right). An LFT treatment results in an uncorrelated picture where electrons are localized at the vanadium (III) metal center, but a [42,40] 2-RDM treatment results in correlated electrons that are entangled throughout the ligand π manifold, where fractional occupation numbers are represented by arrows of different size. 41

4.4 Skeletal structure of bis(ethylene-1,2-dithiolato)nickel, or $Ni(edt_2)$ 51

4.5 Visualized orbitals for the two active spaces in the monoanion with occupation numbers and symmetry below. The larger active space includes the singly occupied $3d_{x^2-y^2}$ orbital, along with two correlated B_{2g} orbitals, which are completely uncorrelated in the smaller active space. 56

4.6 Structures for CrF_6 in octahedral, (a), and trigonal prismatic, (b), conformations 75

4.7 Skeletal structure of $Ni(edt)_2$. 77

4.8 Representative natural orbitals for the $Ni(edt)_2$ complex. The B_{1g} σ-type orbital, (a), and the B_{2g} π-type orbital, (b), play an important role at the occupied-unoccupied gap in the monoanion $Ni(edt)_2$ complex. 78

LIST OF TABLES

4.1 Orbital occupations indicate strong correlation and entanglement in the vanadium (III) complex with the [42,40] active space: a quantitative comparison of the occupations for the highest and lowest occupied molecular (natural) orbitals (HOMO and LUMO) as well as the next highest and next lowest orbitals (HOMO-1 and LUMO+1). While LFT is uncorrelated with HOMO and LUMO occupations of 2 and 0 and the [12,10] set is close to the LFT limit, the [42,40] set is strongly correlated with HOMO and LUMO occupations of 1.372 and 0.258, respectively. 42

4.2 Mulliken charges in the [12,10] and [42,40] sets provide two different pictures of reduction of the vanadium oxo complex. In the [12,10] 2-RDM calculation the decrease in the charge of the vanadium and oxygen atoms is substantial, which is in agreement with ligand-field theory's prediction of a metal-centered reduction. In contrast, the [42,40] 2-RDM calculation predicts a ligand-centered reduction in which the electron is primarily added to the pyridine ligands. The calculations were performed utilizing DQG N-representability conditions. 43

4.3 Natural-Orbital Descriptions for $Ni(edt)_2$ 54

4.4 Ionization Potentials ($E_{\text{final}} - E_{\text{initial}}$) for $Ni(edt)_2$ (kcal/mol) 56

4.5 $Ni(edt)_2$ Ligand Electron Count 57

4.6 $[Ni(edt)_2]^0$ Singlet-Triplet Gap (kcal/mol) 58

4.7 Differences in bond lengths and energies for various methods for two different conformations of CrF_6. The V2RDM result consistently predicts a longer bond than CCSD(T), and predicts a slightly smaller energy difference. 76

4.8 Natural orbital occupations near the occupied-unoccupied gap for the active space RDM calculation and CCSD for the octahedral conformation of CrF_6. All RDM results are from the [42,26] active space. 77

4.9 Selected bond lengths for the $[Ni(edt)_2]^{-1}$ optimized geometries for a [19,13] active space of the D_{2h} and C_1 wavefunctions as well as the C_1 V2RDM solution, and the B3LYP D_{3h} minimum. 79

4.10 Occupation numbers and atomic orbital description for $[Ni(edt)_2]^{-1}$ using a [19,13] active space including all π and nickel $3d$ orbitals. 79

ACKNOWLEDGMENTS

This dissertation would have been impossible without an enormous amount of support from co-workers, family, and friends. My advisor and mentor David Mazziotti allowed me the freedom and time to explore my interests and curiosities, while still providing the guidance necessary to move the research in a positive direction. His personal mentorship in non-academic matters has also been very generous, and for that I am very thankful. Many thanks go to the other members of the Dissertation committee, Professors Tim Berkelbach and John Anderson who gave many good comments and suggestions as well as support. Many past and present members of the Mazziotti group have contributed to this dissertation either directly or indirectly. Chad, Andrew, Nick, Srikant, Erik, Romit, Andrew, and Erica all provided a warm welcome and plenty of advice when I joined the group. Kade, Manas, Ali, Lexie, Shayan, Shiva, Jason, and Scott have all been fantastic co-workers and friendly faces. Greg deserves special thanks for laying important groundwork for the research described here. I have been enormously lucky to have the support of many, many friends at the University of Chicago, and from Berlin, Omaha, and Sioux Falls. I am particularly grateful to my undergraduate advisor, Professor Bradley Parsons for enormous support and encouragement during my time at Creighton University.

Most importantly this dissertation is the result of incredible support from my family: my sisters, Catherine and Elizabeth, and my parents, John and Pat. Whatever I have accomplished is a direct result of their support, and for that I am incredibly grateful. None of this work would have been possible without the support of my family and friends, and they deserve enormous credit. All errors are my own.

ABSTRACT

Accurate calculation of quantum electron correlation effects is essential for understanding the molecular electronic structure of organometallic chemicals. Electron correlation and delocalization contribute to stabilization of chemical species, and provide a mechanism through which non-classical and non-intuitive chemical behaviors occur. Oxidation and reduction of metal complexes, for example, are classically thought to occur at the metal site; stabilization of delocalized electrons throughout the ligand field, however, can allow for ligand-centered redox processes. These ligand-centered processes, known as ligand non-innocence, are central to an emerging area of investigation relevant to the catalysis, chemical transformation, and energy transfer fields. Computation of the correlation effects in these large organometallic species is hindered by the exponential scaling of traditional wavefunction methods which explicitly treat electron correlation. I describe several methods that are based on the two-electron reduced density matrix (2-RDM) that avoid the exponential cost of computing the entire wavefunction. Since the energy of a quantum electronic system is an exact linear functional of the 2-RDM, direct determination of the 2-RDM with respect to the electronic Hamiltonian allows the determination of the energy and correlation effects with polynomially scaling algorithms. This favorable scaling allows for the description of electron correlation for organometallic systems which are far beyond the computational capabilities of traditional wavefunction techniques. I also describe the use of analytical gradient techniques in this methodological context and show how large-scale correlated calculations offer predicted geometries of metal complexes that differ from smaller correlated calculations.

CHAPTER 1

INTRODUCTION

1.1 N-Electron Wavefunction Theory

Molecular electronic structure is described by the time-independent Schrödinger equation,

$$\hat{H}\Psi_n = E\Psi_n, \tag{1.1}$$

where $\hat{H}$, the Hamiltonian, is the sum of one- and two-body interactions,

$$\hat{H} = {}^1\hat{h}(i) + {}^2\hat{V}(i,j). \tag{1.2}$$

The one-body terms, ${}^1\hat{h}$, contain the nuclear-electron repulsion terms as well as the kinetic energy of the electron, and the two-body piece, ${}^2\hat{V}$, contains the electron-electron repulsion term which is inversely proportional to the inter-electron distance. Here we are assuming the Born-Oppenheimer approximation which decouples the motion of the electrons from the nuclei.[1]

The wavefunction, Ψ_n, in Eq. 1.1 describes the electronic state of the molecule. The wavefunction contains all information about the electronic state of the molecule, including the complete excited state spectrum, therefore calculating the wavefunction is the primary goal of electronic structure theory. Computing the wavefunction, however, is challenging because of the difficulty in solving Eq. 1.1; exact solution of the equation scales exponentially with the number of electrons. This scaling is dictated by the two-particle interactions of the ${}^2\hat{V}$ term.

There are many approximations to the solution of the Schrödinger equation, one of the most basic, and fundamental, is the Hartree-Fock approximation. Hartree-Fock is known as a mean-field theory, because instead of solving the electron-electron repulsion exactly, the terms are computed in the average field of the other electrons. Instead of the Hamiltonian

operator in Eq. 1.1 we define the Fock operator which is an effective one-electron potential derived from the total molecular Hamiltonian,

$$\hat{F} = {}^1\hat{h} + {}^1\hat{J} - {}^1\hat{K}, \tag{1.3}$$

where ${}^1\hat{J}$ and ${}^1\hat{K}$ are the Coulomb and exchange operators respectively.[2] Modern implementations of Hartree-Fock theory efficiently scale as $O(r^3)$ where r is the rank of the orbital basis. The Hartree-Fock energy is always an underestimation of the stability of the electronic state, i.e. the predicted energy is too *high*. The energy predicted from the exact solution to the Schrödinger equation will always be exactly equal to or, more commonly, less than the Hartree-Fock solution. Hartree-Fock theory provides a rich framework to view electronic structure theory, but it is lacking a fundamental feature. Hartree-Fock is explicitly formulated as a one-electron picture and neglects the solution to the two-electron part of the molecular electronic Hamiltonian. In spite of this, Hartree-Fock energies almost always recover about 90% of the electronic energy and typically recover over 99% of the electronic energy.

In spite of the success of Hartree-Fock theory at recovering many important features of electronic structure, the lack of a two-electron treatment is a problematic approximation. Even while recovering enormous proportions of the energy with the Fock operator, the two-electron interactions frequently tune the electronic structure of the molecule in a significant way making the one-electron approximation inappropriate. Methods which seek to treat two-electron interactions are generally known as post-Hartree-Fock methods. One of the most fundamental of these methods is known as configuration interaction (CI).[3]

Configuration interaction finds a solution to the Schrödinger equation by computing the interaction between all possible determinants in an orbital basis. Consider the expansion of the wavefunction into of a basis of anti-symmetrized functions, χ_i,

$$\Psi_n = \sum_i c_i \chi_i. \tag{1.4}$$

The basis functions χ_i are in this case determinants which describe the filling of the orbital basis with the electrons. These determinants are in turn expanded in terms of an orbital basis, which are usually contracted Gaussian functions. The Hartree-Fock determinant, for example, is the configuration in which the orbital filling proceeds from most-stable to least-stable until all electrons are in orbitals, and in accordance with the Pauli exclusion principle, which requires that no two electrons share all four quantum numbers. A singly-excited determinant, on the other hand, would move one electron from a low-lying orbital into a previously unoccupied high-lying orbital. Each of these determinants is called a configuration, and the solving for their interactions is called the configuration interaction. If all possible excitations are taken into account, the full configuration interaction (FCI) is computed. FCI is an exact solution to Eq. 1.1, and scales exponentially in system size, $O(r^N)$, where N is the number of electrons and r is the size of the orbital basis. Currently implementations of FCI limit the number of electrons and orbitals to about 18, which is a significant prohibition on system size. One common approach to treating systems of much larger size is through *active space* treatments. These methods choose a particular set of orbitals and electrons to solve exactly through CI, while treating the remaining electrons and orbitals in a less sophisticated fashion, usually with Hartree-Fock. Even in the active space ansatz, the correlated space is still limited to about 18 electrons and orbitals, since the correlated active space is described exactly with the CI. I describe active space methods in Chapter 2.

1.2 Reduced Density Matrix Formalism

The wavefunction contains all information about the molecular electronic state. The N-electron density matrix is the outer product of the N-electron wavefunction with itself,

$$^{N}D = \Psi(1, ..., N)\Psi^{*}(\overline{1}, ..., \overline{N}). \tag{1.5}$$

Integration over all electrons except two yields the two-electron reduced density matrix, or 2-RDM,

$$^{2}D = \binom{N}{2} \int \Psi(1, ..., N)\Psi^{*}(1, ..., N)d3...dN \tag{1.6}$$

The Hamiltonian in Eq. 1.2 is explicitly composed of one-electron and two-electron terms. The Hamiltonian can be expressed as a two-body operator, properly normalized, with,

$$^{2}K = \frac{2}{N-1}\bigg(-\nabla_1^2 - \sum_j \frac{Z_j}{r_{1j}}\bigg) + \frac{1}{2}\frac{1}{r_{12}} \tag{1.7}$$

Finally, because electrons interact pairwise and are indistinguishable, the energy of a electronic system, as in Eq. 1.1, can be written as an exact linear functional of the 2-RDM and ^{2}K,[4]

$$E = \mathrm{Tr}(\ ^{2}K\ ^{2}D). \tag{1.8}$$

From this equation it is clear that determination of the energy of a fermionic quantum system depends only on the 2-RDM, and not the entire wavefunction.[5–7] Techniques which attempt to determine the 2-RDM directly, instead of through explicit integration of the full wavefunction may avoid the exponential complexity of the full wavefunction.[8–18] In Chapter 2 I describe two methods that determine the 2-RDM directly, namely variational 2-RDM (V2RDM) theory[19–25] and the anti-Hermitian contracted Schrödinger equation (ACSE).[26–34]

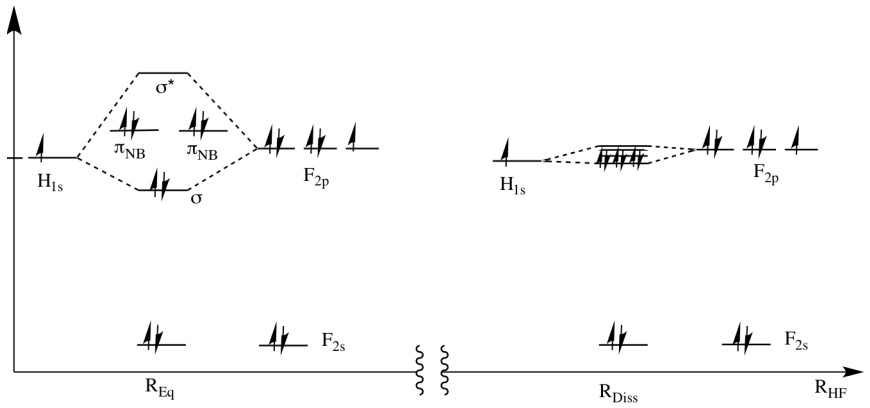

Figure 1.1: Schematic MO's for the dissociation of hydrogen fluoride.

1.3 Electron Correlation

In molecular electronic structure the terms *electron correlation*, and more particularly *two-electron correlation* refer to the pairwise nature of electronic interactions.[35] Hartree-Fock theory treats the two-electron interactions in an average, or mean field description. By the variational theorem, treating the two-electron part of the Hamiltonian beyond mean-field will always lower the energy of the system. These treatments are intended to go beyond the mean-field description of the two-electron energy and provide an approximation of the correlation energy. The exact correlation energy is defined relative to the Hartree-Fock and FCI energies, as in Eq. 1.9.

$$E_{\text{Corr}} = E_{FCI} - E_{HF} \tag{1.9}$$

The correlation energy is defined as a negative quantity, which is evident from the fact that the FCI energy is always less than or equal to the Hartree-Fock energy by the variational theorem. While Equation 1.9 defines the *exact* correlation energy, other methods that do not yield the exact FCI solution will *approximate* the correlation energy.

Two-electron correlation has important effects in single atoms, small molecules, and large complexes. In single atoms for instance, electron correlation is important in understanding the near-degeneracies in the $4s$ and $3d$ orbitals in the first row transition metals.[36] In small

molecules, accurate treatment is required for the dissociation of diatomics like N_2 and HF.[37] Fig. 1.1 schematically shows the dissociation of the HF molecule and the changes to the molecular orbital (MO) diagram. On the left, the diatomic is near the equilibrium geometry, and in this case the MO diagram is dominated by one configuration. On the right, however, near dissociation, the π and σ orbitals become quasidegenerate, and several MO diagrams must be used to characterized the ground state. These MO diagrams, or references, or configurations, all contribute to the overall ground state in the dissociation limit. I show examples of electron correlation in large and complex molecules in detail in Chapter 4. These examples include correlation effects in oxidations of vanadium oxo pyridine structures, nickel dithiolates, as well as the effects of electron correlation on geometry of chromium hexaflouride and titanium, chromium, and zinc diiminoquinonephenolate complexes.[38,39]

1.4 References

(1) McWeeney, R., *Methods of Molecular Quantum Mechanics*; Academic Press: New York, 1989.

(2) Szabo, A.; Ostlund, N. S., *Modern Quantum Chemistry*; Dover: New York, 1989.

(3) Helgaker, T.; Jorgensen, P.; Olsen, J., *Modern Electronic-Structure Theory*; Wiley: New York, 2000.

(4) Mazziotti, D. A. Two-Electron Reduced Density Matrix as the Basic Variable in Many-Electron Quantum Chemistry and Physics. *Chemical Reviews* **2012**, *112*, 244–262.

(5) Coleman, A. J. Structure of Fermion Density Matrices. *Review of Modern Physics* **1963**, *35*, 668–686.

(6) Coleman, A.; Yukalov, V., *Reduced Density Matrices: Coulson's Challenge*; Springer: New York, 2000.

(7) Garrod, C.; Percus, J. K. Reduction of the N-Particle Variational Problem. *Journal of Mathematical Physics* **1964**, *5*, 1756–1776.

(8) Erdahl, R. M. Representability. *International Journal of Quantum Chemistry* **1978**, *13*, 697–718.

(9) Mazziotti, D. A. In *Reduced-Density-Matrix Mechanics: With Application to Many-Electron Atoms and Molecules*, Mazziotti, D. A., Ed.; John Wiley & Sons, Inc.: 2007, pp 19–59.

(10) Zhao, Z.; Braams, B. J.; Fukuda, M.; Overton, M. L.; Percus, J. K. The reduced density matrix method for electronic structure calculations and the role of three-index representability conditions. *Journal of Chemical Physics* **2004**, *120*, 2095–104.

(11) Mazziotti, D. A. Realization of quantum chemistry without wave functions through first-order semidefinite programming. *Physical Review Letters* **2004**, *93*, 213001.

(12) Mazziotti, D. A. First-order semidefinite programming for the direct determination of two-electron reduced density matrices with application to many-electron atoms and molecules. *Journal of Chemical Physics* **2004**, *121*, 10957–66.

(13) Mazziotti, D. A. Variational two-electron reduced density matrix theory for many-electron atoms and molecules: Implementation of the spin- and symmetry-adapted T_2 condition through first-order semidefinite programming. *Physical Review A* **2005**, *72*, 032510.

(14) Mazziotti, D. A.; Erdahl, R. M. Uncertainty relations and reduced density matrices: Mapping many-body quantum mechanics onto four particles. *Physical Review A* **2001**, *63*, 042113.

(15) Mazziotti, D. A. Large-scale semidefinite programming for many-electron quantum mechanics. *Physical Review Letters* **2011**, *106*, 083001.

(16) Mazziotti, D. A. Structure of fermionic density matrices: complete $N-$representability conditions. *Physical Review Letters* **2012**, *108*, 263002.

(17) Mazziotti, D. A. Significant conditions for the two-electron reduced density matrix from the constructive solution of N-representability. *Physical Review A* **2012**, *85*, 062507.

(18) Mazziotti, D. A. Enhanced Constraints for Accurate Lower Bounds on Many-Electron Quantum Energies from Variational Two-Electron Reduced Density Matrix Theory. *Physical Review Letters* **2016**, *117*, 153001.

(19) Shenvi, N.; Izmaylov, A. F. Active-space $N-$representability constraints for variational two-particle reduced density matrix calculations. *Physical Review Letters* **2010**, *105*, 213003.

(20) Nakata, M.; Nakatsuji, H.; Ehara, M.; Fukuda, M.; Nakata, K.; Fujisawa, K. Variational calculations of fermion second-order reduced density matrices by semidefinite programming algorithm. *Journal of Chemical Physics* **2001**, *114*, 8282–8292.

(21) Mazziotti, D. A. Variational minimization of atomic and molecular ground-state energies via the two-particle reduced density matrix. *Physical Review A* **2002**, *65*, 062511.

(22) Gidofalvi, G.; Mazziotti, D. A. Spin and symmetry adaptation of the variational two-electron reduced-density-matrix method. *Physical Review A* **2005**, *72*, 052505.

(23) Hammond, J. R.; Mazziotti, D. A. Variational reduced-density-matrix calculations on radicals: An alternative approach to open-shell *ab initio* quantum chemistry. *Physical Review A* **2006**, *73*, 012509.

(24) Gidofalvi, G.; Mazziotti, D. A. Active-space two-electron reduced-density-matrix method: complete active-space calculations without diagonalization of the $N-$electron Hamiltonian. *Journal of Chemical Physics* **2008**, *129*, 134108.

(25) Van Aggelen, H.; Verstichel, B.; Bultinck, P.; Van Neck, D.; Ayers, P. W. Considerations on describing non-singlet spin states in variational second order density matrix methods. *Journal of Chemical Physics* **2012**, *136*, 014110.

(26) Mazziotti, D. A. Contracted Schrödinger equation: Determining quantum energies and two-particle density matrices without wave functions. *Physical Review A* **1998**, *57*, 4219–4234.

(27) Mazziotti, D. A. Anti-Hermitian contracted Schrödinger equation: direct determination of the two-electron reduced density matrices of many-electron molecules. *Physical Review Letters* **2006**, *97*, 143002.

(28) DePrince, E.; Mazziotti, D. A. Cumulant reconstruction of the three-electron reduced density matrix in the anti-Hermitian contracted Schrödinger equation. *Journal of Chemical Physics* **2007**, *127*, 104104.

(29) Mazziotti, D. A. Anti-Hermitian part of the contracted Schrödinger equation for the direct calculation of two-electron reduced density matrices. *Physical Review A* **2007**, *75*, 022505.

(30) Mazziotti, D. A. Two-electron reduced density matrices from the anti-Hermitian contracted Schrodinger equation: enhanced energies and properties with larger basis sets. *Journal of Chemical Physics* **2007**, *126*, 184101.

(31) Mazziotti, D. A. Multireference many-electron correlation energies from two-electron reduced density matrices computed by solving the anti-Hermitian contracted Schrödinger equation. *Physical Review A* **2007**, *76*, 052502.

(32) Gidofalvi, G.; Mazziotti, D. A. Direct calculation of excited-state electronic energies and two-electron reduced density matrices from the anti-Hermitian contracted Schrödinger equation. *Physical Review A* **2009**, *80*, 022507.

(33) Rothman, A. E.; Foley, J. J.; Mazziotti, D. A. Open-shell energies and two-electron reduced density matrices from the anti-Hermitian contracted Schrödinger equation: A spin-coupled approach. *Physical Review A* **2009**, *80*, 052508.

(34) Sand, A. M.; Mazziotti, D. A. Enhanced computational efficiency in the direct determination of the two-electron reduced density matrix from the anti-Hermitian contracted Schrödinger equation with application to ground and excited states of conjugated π-systems. *Journal of Chemical Physics* **2015**, *143*, 134110.

(35) Mayer, J. E. Electron Correlation. *Physical Review* **1955**, *100*, 1579–1586.

(36) Dunning, T. H.; Botch, B. H.; Harrison, J. F. On the Orbital Description of the 4s3dn+1 States of the Transition Metal Atoms. *Journal of Chemical Physics* **1980**, *72*, 3419–3420.

(37) Chaudhuri, R. K.; Freed, K. F.; Abrash, S. A.; Potts, D. M. A critical comparison of theoretical and experimental electronic spectrum and potential energy curves of HF molecule and its positive and negative ions. *Journal of Molecular Structure: THEOCHEM* **2001**, *547*, 83 –96.

(38) Schlimgen, A. W.; Heaps, C. W.; Mazziotti, D. A. Entangled Electrons Foil Synthesis of Elusive Low-Valent Vanadium Oxo Complex. *Journal of Physical Chemistry Letters* **2016**, *7*, 627–631.

(39) Schlimgen, A. W.; Mazziotti, D. A. Static and Dynamic Electron Correlation in the Ligand Noninnocent Oxidation of Nickel Dithiolates. *Journal of Physical Chemistry A* **2017**, *121*, 9377–9384.

CHAPTER 2

AB INITIO QUANTUM CHEMICAL METHODS FOR COMPUTING ELECTRON CORRELATION

2.1 Introduction

As described in Chapter 1 the FCI solution to all but the most trivial systems is generally intractable due to the r^N scaling of the method. We can modify the FCI method and instead choose a subset of orbitals from the orbital basis and designate this subset the *active space*. We then first, compute the FCI solution for the active space, and then perform orbital rotations in order to lower the energy. This procedure is repeated until a self-consistent solution is achieved. This method is the general procedure of complete active space self-consistent field (CASSCF) theory, which is explained in Section 2.2.

The electronic energy of the molecular electronic Hamiltonian is an exact linear functional of the 2-RDM, therefore computing the energy alone does not require the solution of the entire wavefunction, but only the 2-RDM.[1,2] This applies as well in CASSCF theory, so computation of the correlation energy using the CASSCF method can also be driven by a 2-RDM approach. Variational 2-RDM theory (V2RDM) computes the 2-RDM alone, at polynomial cost instead of the exponential cost of computing the entire wavefunction.[3–17] Using V2RDM correlation energy and other correlation metrics can be computed for much larger systems than using wavefunction driven CASSCF.[18–34] 2-RDM driven CASSCF is described in Section 2.3.

CASSCF gives a description of the static correlation in a molecule, or a description of how multiple electronic configurations contribute to the overall electronic state. Static correlation is related to the degeneracy of electronic configurations. Dynamic correlation, on the other hand, is generally estimated with perturbative techniques. The distinction between static and dynamic correlation is somewhat artificial because the physical correlation energy is exactly determined by the full configuration interaction. On the other hand, methods which

approximate the FCI energy, like perturbation theory and CASSCF, frequently compute correlation energies of different orders of magnitude, so it is clear that the different treatments yield different insight.

Perturbation theory and configuration interaction approaches are also combined for multireference perturbation theory (MRPT).[35–38] MRPT is most frequently used in its second-order form MRPT2. These techniques have many variants to improve scaling and accuracy, but in general the perturbative correction to the energy of a configuration interaction wavefunction is computed. Another approach at computing the so-called dynamic correlation energy is by computing the solution to the anti-Hermitian contracted Schrödinger equation (ACSE), which is an RDM-driven method through the solution of a series of differential equations. Solving the ACSE is known to give energies that are as or more accurate than MRPT2 results.[32,39–58] These methods are briefly described in Section 2.4.

Finally in Section 2.5 I discuss analytical gradient techniques for CASSCF. Analytical gradients are used to compute optimized molecular geometries of different stationary points on the potential energy surface. Importantly, the gradient of the CASSCF energy depends only 2-RDM, and the basis and configuration of the nuclei. I describe the standard derivation of the analytical gradients for CASSCF before describing an alternative derivation using a Cholesky decomposition.

2.2 Complete Active Space Self Consistent Field Theory

The CASSCF method is a size-consistent method which approximates the correlation energy in a quantum system. As noted in previous sections, the solution to FCI scales as $O(r^N)$ which significantly limits the number of orbitals and electrons that can be explicitly correlated. Instead of computing the FCI for the entire orbital space, r, the CASSCF calculation only correlates a subset of orbitals, r_a, called the active orbitals. A FCI calculation is performed spanning the active space, and a subsequent set of orbital rotations are performed to achieve a self-consistent field.[59–61]

CASSCF is an iterative two-step method, and the most common procedure is first the CI calculation followed by the orbital rotation. Even though the CI space is substantially smaller than the full orbital basis, CI calculations in the most advanced traditional implementation can only correlate up to 18 electrons in 18 orbitals. Active spaces of this size are frequently far too small to sufficiently capture the electronic interactions in organometallic and other large molecule chemistry.[62] A significant portion of contemporary correlated electronic structure theory efforts focus on the approximate solution to the CI problem, frequently in the CASSCF ansatz. Examples include density matrix renormalization group (DMRG), restricted active space (RAS) methods, as well as reduced density matrix (RDM) methods described below.[63,64]

2.3 Variational 2-RDM Theory

We use the variational 2-RDM method to approximate the static correlation present in the wavefunction. As with wavefunction CASSCF,[59,60,65] RDM-based CASSCF variationally solves the Schrödinger equation in the active space to account for most of the strong correlation, and then rotates the orbitals to lower the energy until self-consistency.[14,17,18,23,28,66]

The active-space variational 2-RDM method calculates the 2-RDM directly, which avoids the explicit calculation of the entire wavefunction.[7] Thus the 2-RDM method benefits from polynomial scaling in system size, whereas traditional wavefunction CASSCF scales exponentially.[10] While the systems studied here are tractable with wavefunction CASSCF, the current limit for active-space size is about [18,18], which eliminates wavefunction CASSCF as a viable method for studying transition-metal complexes with large active spaces.

The energy of an electronic system is a linear functional of the 2-RDM,

$$E = \mathrm{Tr}(\ {}^2K\ {}^2D), \tag{2.1}$$

where ${}^2D$ is the 2-RDM and ${}^2K$ is the reduced electronic Hamiltonian.[4] We minimize the

energy of a 2-RDM that is constrained to be approximately N-representable by imposing a set of constraints in a semidefinite programming optimization.[10] Since the 2-RDM is not directly contracted from the full wavefunction, we must impose constraints to ensure the N-representability of the 2-RDM:[1]

$$\begin{aligned} {}^2D &\succeq 0 \\ {}^2Q &\succeq 0 \\ {}^2G &\succeq 0 \end{aligned} \tag{2.2}$$

where D, Q, and G matrices are the two-particle, two-hole, and particle-hole matrices respectively, and $M \succeq 0$ indicates that the matrix M is positive semidefinite. A matrix is *positive semidefinite* if and only if its eigenvalues are nonnegative. The 2-positivity (or DQG) conditions ensure that the probability distributions of two particles, two holes, and a particle and a hole are nonnegative.

Beyond the 2-positivity conditions we enforce a subset of three-particle constraints known as the T_2 condition. While the T_2 condition is generated by keeping the sum of two three-particle density matrices positive semidefinite, it can be written explicitly as a linear functional of only the 2-RDM.[5,8,10] Several other constraints are also enforced, including the Hermiticity and antisymmetry of the 2-RDM along with appropriate trace and spin constraints.[8,15] This set of constraints has been shown to give nearly quantitative accuracy in a variety of contexts when compared to wavefunction CASSCF.[5,22] While CASSCF scales exponentially with system size $O(r^N)$, the variational 2-RDM method with D, Q, and G conditions scales as $O(r^6)$ with r being the number of active orbitals and N the number of active electrons. The present paper uses the conventional form of the T_2 condition which scales as $O(r^9)$, but for larger systems a polar-cone formulation of the T_2 condition has been developed which scales as $O(r^6)$.[13]

2.4 Anti-Hermitian Contracted Schrödinger Equation

The 2-RDM from the active-space calculation includes correlation of the active orbitals only. Correlation from the inactive orbitals can be included from a solution to the ACSE, seeded with the 2-RDM from the active-space variational 2-RDM calculation.[40,43–45,48,58] Conventionally, the correlation added by the ACSE would be described as dynamic correlation. ACSE and MRPT2 both describe dynamic correlation in a quantum system; here we use a variant of MRPT2 known as N-electron valence second-order perturbation theory (NEVPT2).[36]

The ACSE can be expressed as

$$\langle\psi|[\hat{a}_i^\dagger \hat{a}_j^\dagger \hat{a}_l \hat{a}_k, \hat{H}]|\psi\rangle = 0, \tag{2.3}$$

where $\hat{H}$ is the electronic Hamiltonian operator, $\hat{a}^\dagger$ and $\hat{a}$ are creation and annihilation operators in second quantization respectively, and the square brackets indicate the commutator.

Rearrangement of the creation and annihilation operators shows that the ACSE depends on the 3-RDM. However, the 3-RDM can be approximated through a cumulant reconstruction with the 1- and 2-RDMs

$${}^3D^{i,k,m}_{j,l,n} \approx {}^1D^i_j \wedge {}^1D^k_l \wedge {}^1D^m_n + 3({}^2D^{i,k}_{j,l} - {}^1D^i_j \wedge {}^1D^k_l) \wedge {}^1D^m_n, \tag{2.4}$$

where $\wedge$ is the Grassmann wedge product.[39,67] While this approximation to the 3-RDM is correct through second order of many-body perturbation theory, the iterative solution of the ACSE incorporates higher orders of perturbation theory in a form of renormalization. An approximation is said to be *size extensive* if and only if the error in its energy and 2-RDM scales linearly with system size. Because the part of the 3-RDM neglected in Eq. (2.4) is the cumulant part, which scales linearly with system size, the error in solving the ACSE with this approximation scales linearly with system size, and hence, the energies and 2-RDMs are

size extensive.[44,58] Multiple spin states can be computed with the ACSE. The initial 2-RDM guess can be chosen from the solution of the target spin state by CASSCF or the variational 2-RDM method. Practically, the ACSE is solved for an improved 2-RDM by a series of unitary transformations that preserve the spin symmetry.[48] The solution to the ACSE scales as $O(r_a^2 r_i^4)$ where r_a and r_i are active and inactive orbitals respectively. Further details of the iterative solution to the ACSE can be found elsewhere.[40,44,48,58]

2.5 Analytical Gradient Techniques for CASSCF

2.5.1 Analytical Gradient of Variational 2-RDM Theory

The energy of a molecular electronic state is a linear functional of the 2-RDM (Eq. 2.1). Minimizing the energy of a given Hamiltonian with respect to the 2-RDM can be achieved through a semi-definite program (SDP) written as

$$\begin{aligned} \underset{{}^2D,M}{\text{minimize}} \quad & E = \mathrm{Tr}({}^2S^{-1}\ {}^2K\ {}^2S^{-1}\ {}^2D) \\ \text{subject to} \quad & {}^2D \succeq 0 \\ & M \succeq 0 \\ & f_i({}^2D, M, {}^2S^{-1}) = b_i. \end{aligned} \tag{2.5}$$

The matrix M is the metric matrix which enforces the positivity of the particle-hole and hole-hole matrices introduced above, and ${}^2D$ and ${}^2K$ are expressed in the atomic orbital basis. The objective, E, is minimized subject to the set of linear equalities, $f_i = b_i$. The tensor ${}^2S^{-1}$ is the antisymmetric product of the inverse overlap matrix with itself. The overlap matrix is required since Eq. 2.1 holds only if the basis is orthonormal. The gradient of Eq. 2.5 is seemingly non-trivial because, while the 2-RDM is stationary at the minimum, the overlap matrix need not be.

This difficulty can be over come by modifying the SDP in Eq. 2.5 as,

$$\begin{aligned} \underset{{}^2D,M}{\text{minimize}} \quad & E = \mathrm{Tr}({}^2\bar{K}\,{}^2\bar{D}) \\ \text{subject to} \quad & {}^2\bar{D} \succeq 0 \\ & \bar{M} \succeq 0 \\ & \bar{f}_i({}^2\bar{D}, \bar{M}) = \bar{b}_i. \end{aligned} \tag{2.6}$$

In Eq. 2.6 we have transformed the 2-RDM and the reduced Hamiltonian using the relations,

$$\begin{aligned} {}^2S^{-1} &= {}^2L\ {}^2L^T \\ {}^2\bar{K} &= {}^2L^T\ {}^2K\ {}^2L \\ {}^2\bar{D} &= {}^2L^T\ {}^2D\ {}^2L. \end{aligned} \tag{2.7}$$

Here we have used a Cholesky decomposition of the inverse overlap matrix to compute a lower triangular matrix, L. This formulation of the SDP minimizes the objective with respect to ${}^2\bar{D}$ and so ensures that ${}^2\bar{D}$ is stationary with respect to infinitesimal changes in the nuclear coordinates. This approach is conceptually similar to that of Helgaker and Almlöf, except that our formulation avoids all reference to the molecular orbitals, and generates the transformation from the Cholesky decomposition of the overlap matrix.[68] The overlap matrix is invertible, so the inverse overlap matrix is positive definite, which implies that the Cholesky decomposition of the inverse overlap matrix is unique. The gradient can therefore be written in a manner which is similar to the Hellmann-Feynman theorem.

Theorem 1.

$$\frac{\partial E}{\partial R} = \mathrm{Tr}\left(\frac{\partial\ {}^2\bar{K}}{\partial R}\ {}^2\bar{D}\right) \tag{2.8}$$

Proof. Differentiating the energy with respect to a nuclear coordinate, R,

$$\begin{aligned}\frac{\partial E}{\partial R} &= \mathrm{Tr}\left(\frac{\partial\ {}^2\bar{K}}{\partial R}\ {}^2\bar{D}\right) + \mathrm{Tr}\left(\ {}^2\bar{K}\frac{\partial\ {}^2\bar{D}}{\partial R}\right) \\ &= \mathrm{Tr}\left(\frac{\partial\ {}^2\bar{K}}{\partial R}\ {}^2\bar{D}\right),\end{aligned} \tag{2.9}$$

where the second term of the chain rule vanishes because the energy is stationary with respect to ${}^2\bar{D}$,

$$\frac{\partial E}{\partial\ {}^2\bar{D}} = 0. \tag{2.10}$$

□

Furthermore, the gradient of the energy can then be written in terms of the gradient of the overlap matrix and the gradient of the Hamiltonian.

Theorem 2. *The gradient of the electronic energy can be written in terms of the gradients of the overlap matrix and the Hamiltonian,*

$$\frac{\partial E}{\partial R} = \mathrm{Tr}\left(\left[\frac{\partial\ {}^2L^T}{\partial R}\ {}^2K\ {}^2L + \text{transpose} +\ {}^2L^T\frac{\partial^2 K}{\partial R}\ {}^2L\right]{}^2\bar{D}\right) \tag{2.11}$$

where

$$\frac{\partial\ {}^2L}{\partial R} = -\ {}^2L\hat{\pi}\left({}^2L^T\frac{\partial\ {}^2S}{\partial R}\ {}^2L\right), \tag{2.12}$$

and π operates on a matrix, maintains the lower triangular portion of the matrix and halves the diagonal, and the gradient of ${}^2L$ is symmetric.

Proof. The gradient of the energy expressed in Eq. 2.8 depends on the nuclear gradient of ${}^2\bar{K}$, which can be expressed in terms of the gradients of the overlap matrix and Hamiltonian,

$$\frac{\partial\ {}^2\bar{K}}{\partial R} = \frac{\partial}{\partial R}\left(\ {}^2L^T\ {}^2K\ {}^2L\right) = \frac{\partial\ {}^2L^T}{\partial R}\ {}^2K\ {}^2L + \text{transpose} +\ {}^2L^T\frac{\partial\ {}^2K}{\partial R}\ {}^2L. \tag{2.13}$$

Substitution into Eq. 2.9 yields Eq. 2.11.

Using the equations of motion of the orthogonality condition and the Cholesky decomposition[69] and rearranging, one arrives at Eq. 2.12,

$$\begin{aligned}\frac{\partial\ {}^2S^{-1}}{\partial R} &= -\ {}^2S^{-1}\frac{\partial\ {}^2S}{\partial R}\ {}^2S^{-1} \\ \frac{\partial\ {}^2S^{-1}}{\partial R} &= \frac{\partial\ {}^2L}{\partial R}\ {}^2L^T + L\frac{\partial\ {}^2L^T}{\partial R}.\end{aligned} \tag{2.14}$$

□

2.5.2 Analytical Gradient for CI Wavefunctions

Analytical gradients for electronic wavefunctions are practical for computing stationary points in the nuclear potential energy surface. Geometry optimization with CI gradients yield insight into the effect of strong correlation on nuclear geometry, and has wide-spread use.[70–76] Gradients for CASSCF have also been used in the RDM context to study many small molecules and pentacene,[77] and analytical response theories and gradients for closely related methods like density-matrix renormalization group (DMRG)[78,79] natural orbital functional theory are also known.[80,81]

The nuclear gradient for the electronic part of CI wavefunction, in the molecular orbital basis, is

$$\frac{\partial \mathrm{E}}{\partial \mathrm{R}} = \sum_{ij}\frac{\partial^1 K^i_j}{\partial \mathrm{R}}\ {}^1D^i_j + \sum_{ijkl}\frac{\partial\ {}^2V^{ij}_{kl}}{\partial \mathrm{R}}\ {}^2D^{ij}_{kl} - \sum_{ij}\frac{\partial S^i_j}{\partial \mathrm{R}}X^i_j, \tag{2.15}$$

Where the first term depends on the derivatives of the one-electron integrals and the 1-RDM and the second term depends on the derivatives of two-electron integrals and the 2-RDM. If the CASSCF wavefunction is stationary with respect to all orbital rotations, the term X^i_j can be written in terms of the one- and two-electron integrals of the initial geometry as well as the RDMs,

$$X_j^i = \sum_k {}^1K_k^i {}^1D_j^k + 2\sum_{klm} {}^2V_{ml}^{ik} {}^2D_{ml}^{jr}. \tag{2.16}$$

The conditions for Eq. 2.16 are always met in a FCI calculation. For a CASSCF calculation these conditions are met when all orbitals are optimized during the orbital rotation step, i.e. no orbitals are frozen.[82] The use of frozen orbitals requires the solution to the couple-perturbed Hartree-Fock equations.[83] All calculations in this paper are performed with no frozen orbitals. Because the Lagrangian of the SDP is stationary with respect to nuclear perturbations in the 2-RDM, we can use the V2RDM method to calculate the gradient of CASSCF wavefunctions with large active spaces.[77]

This formulation of the gradient is similar to the formulation presented in the previous section. In both cases, the gradient depends on the derivative of the Hamiltonian, as well as the derivative of the overlap matrix. In our formulation, however, the derivative of the overlap matrix is explicitly incorporated in the Hamiltonian by the Cholesky decomposition transformations.

2.6 References

(1) Coleman, A. J. Structure of Fermion Density Matrices. *Review of Modern Physics* **1963**, *35*, 668–686.

(2) Coleman, A.; Yukalov, V., *Reduced Density Matrices: Coulson's Challenge*; Springer: New York, 2000.

(3) Erdahl, R. M. Representability. *International Journal of Quantum Chemistry* **1978**, *13*, 697–718.

(4) Mazziotti, D. A. In *Reduced-Density-Matrix Mechanics: With Application to Many-Electron Atoms and Molecules*, Mazziotti, D. A., Ed.; John Wiley & Sons, Inc.: 2007, pp 19–59.

(5) Zhao, Z.; Braams, B. J.; Fukuda, M.; Overton, M. L.; Percus, J. K. The reduced density matrix method for electronic structure calculations and the role of three-index representability conditions. *Journal of Chemical Physics* **2004**, *120*, 2095–104.

(6) Mazziotti, D. A. Realization of quantum chemistry without wave functions through first-order semidefinite programming. *Physical Review Letters* **2004**, *93*, 213001.

(7) Mazziotti, D. A. First-order semidefinite programming for the direct determination of two-electron reduced density matrices with application to many-electron atoms and molecules. *Journal of Chemical Physics* **2004**, *121*, 10957–66.

(8) Mazziotti, D. A. Variational two-electron reduced density matrix theory for many-electron atoms and molecules: Implementation of the spin- and symmetry-adapted T_2 condition through first-order semidefinite programming. *Physical Review A* **2005**, *72*, 032510.

(9) Mazziotti, D. A.; Erdahl, R. M. Uncertainty relations and reduced density matrices: Mapping many-body quantum mechanics onto four particles. *Physical Review A* **2001**, *63*, 042113.

(10) Mazziotti, D. A. Large-scale semidefinite programming for many-electron quantum mechanics. *Physical Review Letters* **2011**, *106*, 083001.

(11) Mazziotti, D. A. Structure of fermionic density matrices: complete $N-$representability conditions. *Physical Review Letters* **2012**, *108*, 263002.

(12) Mazziotti, D. A. Significant conditions for the two-electron reduced density matrix from the constructive solution of N-representability. *Physical Review A* **2012**, *85*, 062507.

(13) Mazziotti, D. A. Enhanced Constraints for Accurate Lower Bounds on Many-Electron Quantum Energies from Variational Two-Electron Reduced Density Matrix Theory. *Physical Review Letters* **2016**, *117*, 153001.

(14) Mazziotti, D. A. Variational minimization of atomic and molecular ground-state energies via the two-particle reduced density matrix. *Physical Review A* **2002**, *65*, 062511.

(15) Gidofalvi, G.; Mazziotti, D. A. Spin and symmetry adaptation of the variational two-electron reduced-density-matrix method. *Physical Review A* **2005**, *72*, 052505.

(16) Hammond, J. R.; Mazziotti, D. A. Variational reduced-density-matrix calculations on radicals: An alternative approach to open-shell *ab initio* quantum chemistry. *Physical Review A* **2006**, *73*, 012509.

(17) Nakata, M.; Nakatsuji, H.; Ehara, M.; Fukuda, M.; Nakata, K.; Fujisawa, K. Variational calculations of fermion second-order reduced density matrices by semidefinite programming algorithm. *Journal of Chemical Physics* **2001**, *114*, 8282–8292.

(18) Gidofalvi, G.; Mazziotti, D. A. Active-space two-electron reduced-density-matrix method: complete active-space calculations without diagonalization of the $N-$electron Hamiltonian. *Journal of Chemical Physics* **2008**, *129*, 134108.

(19) Gidofalvi, G.; Mazziotti, D. A. Application of variational reduced-density-matrix theory to organic molecules. *Journal of Chemical Physics* **2005**, *122*, 094107.

(20) Hammond, J. R.; Mazziotti, D. A. Variational reduced-density-matrix calculation of the one-dimensional Hubbard model. *Physical Review A* **2006**, *73*, 062505.

(21) Gidofalvi, G.; Mazziotti, D. A. Computation of dipole, quadrupole, and octupole surfaces from the variational two-electron reduced density matrix method. *Journal of Chemical Physics* **2006**, *125*, 144102.

(22) Gidofalvi, G.; Mazziotti, D. A. Molecular properties from variational reduced-density-matrix theory with three-particle N-representability conditions. *Journal of Chemical Physics* **2007**, *126*, 024105.

(23) Gidofalvi, G.; Mazziotti, D. A. Multireference self-consistent-field energies without the many-electron wave function through a variational low-rank two-electron reduced-density-matrix method. *Journal of Chemical Physics* **2007**, *127*, 244105.

(24) Rothman, A. E.; Mazziotti, D. A. Variational reduced-density-matrix theory applied to the electronic structure of few-electron quantum dots. *Physical Review A* **2008**, *78*, 032510.

(25) Verstichel, B.; van Aggelen, H.; Van Neck, D.; Ayers, P. W.; Bultinck, P. Variational determination of the second-order density matrix for the isoelectronic series of beryllium, neon, and silicon. *Physical Review A* **2009**, *80*, 032508.

(26) Van Aggelen, H.; Verstichel, B.; Bultinck, P.; Van Neck, D.; Ayers, P. W.; Cooper, D. L. Chemical verification of variational second-order density matrix based potential energy surfaces for the N_2 isoelectronic series. *Journal of Chemical Physics* **2010**, *132*, 114112.

(27) Greenman, L.; Mazziotti, D. A. Strong electron correlation in the decomposition reaction of dioxetanone with implications for firefly bioluminescence. *Journal of Chemical Physics* **2010**, *133*, 164110.

(28) Shenvi, N.; Izmaylov, A. F. Active-space $N-$representability constraints for variational two-particle reduced density matrix calculations. *Physical Review Letters* **2010**, *105*, 213003.

(29) Pelzer, K.; Greenman, L.; Gidofalvi, G.; Mazziotti, D. A. Strong Correlation in Acene Sheets from the Active-Space Variational Two-Electron Reduced Density Matrix Method: Effects of Symmetry and Size. *Journal of Physical Chemistry A* **2011**, *115*, 5632–5640.

(30) Van Aggelen, H.; Verstichel, B.; Bultinck, P.; Van Neck, D.; Ayers, P. W. Considerations on describing non-singlet spin states in variational second order density matrix methods. *Journal of Chemical Physics* **2012**, *136*, 014110.

(31) Schlimgen, A. W.; Heaps, C. W.; Mazziotti, D. A. Entangled Electrons Foil Synthesis of Elusive Low-Valent Vanadium Oxo Complex. *Journal of Physical Chemistry Letters* **2016**, *7*, 627–631.

(32) Schlimgen, A. W.; Mazziotti, D. A. Static and Dynamic Electron Correlation in the Ligand Noninnocent Oxidation of Nickel Dithiolates. *Journal of Physical Chemistry A* **2017**, *121*, 9377–9384.

(33) McIssac, A. R.; Mazziotti, D. A. Ligand non-innocence and strong correlation in manganese superoxide dismutase mimics. *Physical Chemistry Chemical Physics* **2017**, *19*, 4656.

(34) Valentine, A. J. S.; Talapin, D. V.; Mazziotti, D. A. Orbitals, Occupation Numbers, and Band Structure of Short One-Dimensional Cadmium Telluride Polymers. *Journal of Physical Chemistry A* **2017**, *121*, 3142–3147.

(35) Roos, B. O.; Andersson, K. Multiconfigurational perturbation theory with level shift — the Cr_2 potential revisited. *Chemical Physics Letters* **1995**, *245*, 215 –223.

(36) Angeli, C.; Cimiraglia, R.; Malrieu, J.-P. N-electron valence state perturbation theory: A spinless formulation and an efficient implementation of the strongly contracted and of the partially contracted variants. *Journal of Chemical Physics* **2002**, *117*, 9138–9153.

(37) Angeli, C.; Pastore, M.; Cimiraglia, R. New perspectives in multireference perturbation theory: the n-electron valence state approach. *Theoretical Chemistry Accounts: Theory, Computation, & Modeling* **2007**, *117*, 743 –754.

(38) Sokolov, A. Y.; Chan, G. K.-L. A time-dependent formulation of multi-reference perturbation theory. *Journal of Chemical Physics* **2016**, *144*, 064102.

(39) Mazziotti, D. A. Contracted Schrödinger equation: Determining quantum energies and two-particle density matrices without wave functions. *Physical Review A* **1998**, *57*, 4219–4234.

(40) Mazziotti, D. A. Anti-Hermitian contracted Schrödinger equation: direct determination of the two-electron reduced density matrices of many-electron molecules. *Physical Review Letters* **2006**, *97*, 143002.

(41) Mazziotti, D. A. Determining the Energy Gap between the Cis and Trans Isomers of HO_3^- Using Geometry Optimization within the Anti-Hermitian Contracted Schrödinger and Coupled Cluster Methods. *Journal of Physical Chemistry A* **2007**, *111*, 12635–12640.

(42) DePrince, E.; Mazziotti, D. A. Cumulant reconstruction of the three-electron reduced density matrix in the anti-Hermitian contracted Schrödinger equation. *Journal of Chemical Physics* **2007**, *127*, 104104.

(43) Mazziotti, D. A. Anti-Hermitian part of the contracted Schrödinger equation for the direct calculation of two-electron reduced density matrices. *Physical Review A* **2007**, *75*, 022505.

(44) Mazziotti, D. A. Two-electron reduced density matrices from the anti-Hermitian contracted Schrodinger equation: enhanced energies and properties with larger basis sets. *Journal of Chemical Physics* **2007**, *126*, 184101.

(45) Mazziotti, D. A. Multireference many-electron correlation energies from two-electron reduced density matrices computed by solving the anti-Hermitian contracted Schrödinger equation. *Physical Review A* **2007**, *76*, 052502.

(46) Foley, J. J.; Rothman, A. E.; Mazziotti, D. A. Activation energies of sigmatropic shifts in propene and acetone enolate from the anti-Hermitian contracted Schrödinger equation. *Journal of Chemical Physics* **2009**, *130*, 184112.

(47) Gidofalvi, G.; Mazziotti, D. A. Direct calculation of excited-state electronic energies and two-electron reduced density matrices from the anti-Hermitian contracted Schrödinger equation. *Physical Review A* **2009**, *80*, 022507.

(48) Rothman, A. E.; Foley, J. J.; Mazziotti, D. A. Open-shell energies and two-electron reduced density matrices from the anti-Hermitian contracted Schrödinger equation: A spin-coupled approach. *Physical Review A* **2009**, *80*, 052508.

(49) Rothman, A. E.; Mazziotti, D. A. Nonequilibrium, steady-state electron transport with N-representable density matrices from the anti-Hermitian contracted Schrödinger equation. *Journal of Chemical Physics* **2010**, *132*, 104112.

(50) Greenman, L.; Mazziotti, D. A. Energy Barriers of Vinylidene Carbene Reactions from the Anti-Hermitian Contracted Schrödinger Equation. *Journal of Physical Chemistry A* **2010**, *114*, 583–588.

(51) Snyder, J. W.; Rothman, A. E.; Foley, J. J.; Mazziotti, D. A. Conical intersections in triplet excited states of methylene from the anti-Hermitian contracted Schrödinger equation. *Journal of Chemical Physics* **2010**, *132*, 154109.

(52) Foley 4th, J. J.; Rothman, A. E.; Mazziotti, D. A. Strongly correlated mechanisms of a photoexcited radical reaction from the anti-Hermitian contracted Schrödinger equation. *Journal of Chemical Physics* **2011**, *134*, 034111.

(53) Snyder, J. W.; Mazziotti, D. A. Photoexcited conversion of gauche-1,3-butadiene to bicyclobutane via a conical intersection: Energies and reduced density matrices from the anti-Hermitian contracted Schrödinger equation. *Journal of Chemical Physics* **2011**, *135*, 024107.

(54) Snyder, J. W.; Mazziotti, D. A. Conical Intersection of the Ground and First Excited States of Water: Energies and Reduced Density Matrices from the Anti-Hermitian Contracted Schrödinger Equation. *Journal of Physical Chemistry A* **2011**, *115*, 14120–14126.

(55) Greenman, L.; Mazziotti, D. A. Balancing single- and multi-reference correlation in the chemiluminescent reaction of dioxetanone using the anti-Hermitian contracted Schrödinger equation. *Journal of Chemical Physics* **2011**, *134*, 174110.

(56) Sand, A. M.; Schwerdtfeger, C. A.; Mazziotti, D. A. Strongly correlated barriers to rotation from parametric two-electron reduced-density-matrix methods in application to the isomerization of diazene. *Journal of Chemical Physics* **2012**, *136*, 034112.

(57) Snyder, J. W.; Mazziotti, D. A. Photoexcited tautomerization of vinyl alcohol to acetylaldehyde via a conical intersection from contracted Schrodinger theory. *Physical Chemistry Chemical Physics* **2012**, *14*, 1660–1667.

(58) Sand, A. M.; Mazziotti, D. A. Enhanced computational efficiency in the direct determination of the two-electron reduced density matrix from the anti-Hermitian contracted Schrödinger equation with application to ground and excited states of conjugated π-systems. *Journal of Chemical Physics* **2015**, *143*, 134110.

(59) Siegbahn, P. E. M.; Almlöf, J.; Heiberg, A.; Roos, B. O. The complete active space SCF (CASSCF) method in a Newton–Raphson formulation with application to the HNO molecule. *Journal of Chemical Physics* **1981**, *74*, 2384–2396.

(60) Roos, B. O.; Taylor, P. R.; Siegbahn, P. E. A complete active space SCF method (CASSCF) using a density matrix formulated super-CI approach. *Chemical Physics* **1980**, *48*, 157 –173.

(61) Roos, B. O. In *Ab Initio Methods in Quantum Chemistry II*, Lawley, K., Ed.; Advances in Chemical Physics 69; Wiley: New York, 1987, pp 399–446.

(62) Pierloot, K. In *Computational Organometallic Chemistry*, Cundari, T. R., Ed.; Marcel Dekker: 2001; Chapter 5, pp 123–158.

(63) Schollwöck, U. The density-matrix renormalization group. *Review of Modern Physics* **2005**, *77*, 259–315.

(64) Olsen, J.; Roos, B. O.; Jørgensen, P.; Jensen, H. J. A. Determinant based configuration interaction algorithms for complete and restricted configuration interaction spaces. *Journal of Chemical Physics* **1988**, *89*, 2185–2192.

(65) Siegbahn, P.; Heiberg, A.; Roos, B.; Levy, B. A Comparison of the Super-CI and the Newton-Raphson Scheme in the Complete Active Space SCF Method. *Physica Scripta* **1980**, *21*, 323–327.

(66) Cancès, E.; Stoltz, G.; Lewin, M. The electronic ground-state energy problem: a new reduced density matrix approach. *Journal of Chemical Physics* **2006**, *125*, 64101.

(67) Slebodzinski, W., *Exterior Forms and Their Applications*; Polish Scientific Publishers: Warsaw, 1970.

(68) Helgaker, T. U.; Almlöf, J. A secondquantization approach to the analytical evaluation of response properties for perturbationdependent basis sets. *International Journal of Quantum Chemistry*, *26*, 275–291.

(69) Murray, I. Differentiation of the Cholesky Decomposition. *arXiv* **2016**, arXiv:1602.07527.

(70) Szalay, P. G.; Müller, T.; Gidofalvi, G.; Lischka, H.; Shepard, R. Multiconfiguration Self-Consistent Field and Multireference Configuration Interaction Methods and Applications. *Chemical Reviews* **2012**, *112*, 108–181.

(71) Pulay, P. In *Ab Initio Methods in Quantum Chemistry*, Lawley, K., Ed.; Wiley: 1987.

(72) Pulay, P. In *Modern Electronic Structure Theory Part 2*, Yarkony, D., Ed.; World Scientific: 1995.

(73) Taylor, P. R. Analytical MCSCF energy gradients: Treatment of symmetry and CASSCF applications to propadienone. *Journal of Computational Chemistry* **1984**, *5*, 589–597.

(74) Schlegel, H. B. In *Modern Electronic Structure Theory Part 2*, Yarkony, D., Ed.; World Scientific: 1995.

(75) Dupuis, M.; King, H. F. Molecular symmetry. II. Gradient of electronic energy with respect to nuclear coordinates. *Journal of Chemical Physics* **1978**, *68*, 3998–4004.

(76) Shepard, R. In *Modern Electronic Structure Theory Part 2*, Yarkony, D., Ed.; World Scientific: 1995.

(77) Maradzike, E.; Gidofalvi, G.; Turney, J. M.; Schaefer, H. F.; DePrince, A. E. Analytic Energy Gradients for Variational Two-Electron Reduced-Density-Matrix-Driven Complete Active Space Self-Consistent Field Theory. *Journal of Chemical Theory and Computation* **2017**, *13*, 4113–4122.

(78) Dorando, J. J.; Hachmann, J.; Chan, G. K.-L. Analytic response theory for the density matrix renormalization group. *Journal of Chemical Physics* **2009**, *130*, 184111.

(79) Nakatani, N.; Guo, S. Density matrix renormalization group (DMRG) method as a common tool for large active-space CASSCF/CASPT2 calculations. *Journal of Chemical Physics* **2017**, *146*, 094102.

(80) Mitxelena, I.; Piris, M. Analytic gradients for natural orbital functional theory. *Journal of Chemical Physics* **2017**, *146*, 014102.

(81) Mitxelena, I.; Piris, M. Analytic second-order energy derivatives in natural orbital functional theory. *Journal of Mathematical Chemistry* **2018**.

(82) Yamaguchi, Y.; Osamura, Y.; Goddard, J. D.; Schaefer, H. F., *A New Dimension to Quantum Chemistry: Analytical Derivative Methods in Ab Initio Molecular Electronic Structure Theory*; Oxford University Press: 1994.

(83) Osamura, Y.; Yamaguchi, Y.; III, H. F. S. Generalization of analytic configuration interaction (CI) gradient techniques for potential energy hypersurfaces, including a solution to the coupled perturbed Hartree–Fock equations for multiconfiguration SCF molecular wave functions. *Journal of Chemical Physics* **1982**, *77*, 383–390.

CHAPTER 3

ELECTRONIC STRUCTURE METHODS FOR ORGANOMETALLIC CHEMISTRY

3.1 Introduction

Molecules constituted of both metals and organic components are known as organometallic molecules; the organic substructures are generally known as *ligands*. Organometallic chemistry is of significant experimental and theoretical interest. The field of catalysis, in particular, has greatly benefited from a better understanding of the electronic structure of organometallic compounds. Examples of organometallic catalysis include olefin transformation, nitrogen fixation, CO_2 reduction, and water splitting. Organometallic molecules inherit their robust and diverse electronic structures from the combination of the metal center with the unique properties of the ligands. In metal chemistry, the metal-ligand orbital interactions dictate the nature of the frontier orbitals, and therefore strongly influence the reactivity and optical and electronic behavior of metallic complexes.

In this Chapter I describe several methodologies of varying sophistication that describe the electronic structure of organometallic chemistry. First I describe ligand field theory (LFT), which provides a generally accurate first-approximation to qualitative orbital interactions. While LFT can be quantitative, it is not well equipped to describe situations where two-electron interactions are important. Well-understood concepts like backbonding, and electron donation are nonetheless useful in providing an intuitive accounting of the electronic structure.

Next I describe several theoretical methods used for computing properties of organometallic complexes. Historically density functional theory (DFT) has been very widely used to study these complexes. Many years of DFT research in this field has clarified myriad issues in the theoretical treatment of these complexes, including basis set considerations, relativistic effects in the heavier metals, and the behavior of highly charged complexes. DFT benefits

from very favorable computational scaling, and so many properties can be approximated by a skilled DFT practitioner.

Finally, I describe *ab initio* methods in treating organometallic complexes. These treatments have been applied more recently due to the relatively expensive computational cost compared to DFT. We will see, however, that this increase in cost can be essential to describe the electronic structure of organometallics. While DFT includes some treatment of electron correlation, it is not systematic in the way some *ab initio* methods are, and this can yield inconsistent results. *Ab initio* methods include the systematic treatment of electron correlation, which can influence the electronic structure of organometallics to such an extent that the intuitive picture from LFT and the quantitative picture from DFT can be inaccurate.

3.2 Ligand Field Theory

Ligand field theory (LFT) provides many of the basic concepts in describing organometallic chemistry.[1,2] Three such fundamental concepts are the field splitting parameter, σ-donation, and π-backbonding. Each describes how the metal and ligand orbitals interact and gives a qualitative picture for how to describe the orbitals and electron distribution in organometallic molecules.

The central idea of LFT is that the metal atom's d orbitals should dominate the molecular orbital frontier. In the presence of the ligands' electronic structure, the ligand field, the otherwise degenerate set of five d orbitals split in various ways and become non-degenerate. The way the d orbitals split is depends on how the ligand and metal orbitals mix, and this in turn effects the electronic filling for the frontier orbitals. The field splitting parameter, Δ, is used to predict the electronic filling of the d orbitals. Consider an arbitrary octahedral complex ML_6 with four d electrons, where M is the metal and L is the ligand (Figure 3.1). On the left the field splitting parameter is small, so the higher energy e_g orbitals are accessible to the fourth electron, in contrast to the right side with large field splitting parameter. If Δ is large relative to the pairing energy of two electrons, the complex will preferentially take

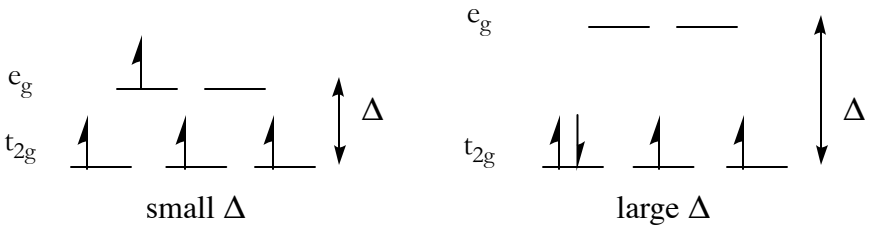

Figure 3.1: Ligand field splitting for ML_6 with two different field splitting parameters, Δ

on a "low-spin" configuration with only two unpaired electrons. In the case of small Δ, the complex will take on the "high-spin" configuration. In this example a small Δ results in all four spins unpaired. Ligand splitting parameters are generally useful at predicting the spin-state of metal-ligand complexes, as demonstrated by the spectrochemical series of ligands and metals.

Beyond predicting the spin-state of a complex, LFT can also describe the relative electron distribution in a complex, and thus yield a qualitative picture of the strength of the bonds in the molecule. Two effects, σ-donation and π-backbonding give indications about how the electron distribution will change based on orbital interaction effects.

When a ligand like NH_3 binds to a metal center, the lone pair on the nitrogen is used to bond with the metal. Since both electrons came from the ligand, NH_3 is described as a σ-donor. Since they are donating electrons, σ-donors generally increase electron density on the metal. A similar situation arises with π-donating ligands, although due to symmetry the donation generally occurs in the t_{2g} orbitals, which are are the same symmetry of π-type orbitals.

Finally, π-backbonding also effects the electron distribution and bonding situation in metallic complexes. Several things are generally necessary in order for this backbonding to occur. First, the metals should be relatively electron rich, second, the ligand π-bonding orbitals should be very stable relative to the metal d orbitals, and finally the ligand π-antibonding orbitals should be able to mix with the metal d orbitals. In this way, the metal t_{2g} orbitals are stabilized through mixing with the π^* orbitals. At the same time, however, since more electron density now occupies the ligand π^* orbitals by virtue of their mixing

with the d orbitals, the π bond in the ligand becomes weaker.

Ligand field splitting, σ-donation, and π-backbonding provide good first approximations to spin-states, orbital mixing, and electron distribution in simple metal complexes. On the other hand, the degree and nature of orbital mixing can be extremely non-intuitive in organometallic complexes, generally because of the presence of extended π-bonded ligands. The ligand field splits the degeneracy of the metal d orbitals, and this effect is the groundwork for ligand field theory; degeneracies, however, can also be introduced by this same interaction. When many π and π^* orbitals in an organometallic complex interact with the metal d orbitals, complicated sets of degenerate or near-degenerate orbitals can arise. In these cases LFT is unable to provide a reliable quantitative description, so more accurate quantum chemical methods must be used instead.

3.3 Density Functional Theory and *ab initio* Methods

The electronic description of organometallic molecules faces a challenge from the outset due to the typical size of those molecules. Conjugated ring systems and other substituent groups along with the metal center results in molecules with many heavy atoms. Furthermore, the complicated electronic structure of these complexes generally requires the use of non-minimal basis sets for an accurate description. Because of this organometallic computational chemistry has grappled with these size constraints.[3]

Density functional theory (DFT) is typically used to describe these compounds.[4–8] DFT is essentially a one-electron picture with the added component of the electronic exchange-correlation.[9] DFT also benefits from favorable scaling in system size, which allows for treatment of large molecules in large basis sets. Furthermore, DFT is generally packaged as a black-box program which allows for experimentalists and other non-computational specialists to approach these molecules in a first-approximation. Specialized applications of DFT can provide insight into other properties of organometallic complexes. Optical and magnetic properties are of particular interest to the experimental community, and DFT applications

can provide accurate results in these contexts, provided sufficient care is taken by the practitioner.

Where DFT scales favorably with respect to system size, another class of methods called *ab initio* methods scale less favorably. As explained in Chapter 1 the full configuration interaction (FCI) scheme scales exponentially in system size, but gives the exact solution to the electronic Schrödinger equation. The complete active space self-consistent field (CASSCF) method, and the 2-RDM implementation of this method, are approximations to the FCI scheme. Increasing the size of the active space yields a better approximation to the exact (FCI) solution. In this way *ab initio* CASSCF is *systematically* improvable in a way that DFT is not. For this reason, CASSCF is a more suitable method in systematically describing the effects of electronic correlation in molecules compared to DFT. While DFT is inexpensive and does provide some insight into the electron correlation, FCI and similar ansätzen provide a systematic framework to understand electron correlation.

3.4 References

(1) Crabtree, R. H., *The Organometallic Chemistry of the Transition Metals*; John Wiley and Sons: New York, 2001.

(2) Spessard, G. O.; Miessler, G. L., *Organometallic Chemistry*; Oxford: New York, 2010.

(3) *Computational Organometallic Chemistry*; Cundari, T. R., Ed.; Marcel Dekker: New York, 2001.

(4) Sperger, T.; Sanhueza, I. A.; Kalvet, I.; Schoenebeck, F. Computational Studies of Synthetically Relevant Homogeneous Organometallic Catalysis Involving Ni, Pd, Ir, and Rh: An Overview of Commonly Employed DFT Methods and Mechanistic Insights. *Chemical Reviews* **2015**, *115*, 9532–9586.

(5) Ghosh, A. Electronic Structure of Corrole Derivatives: Insights from Molecular Structures, Spectroscopy, Electrochemistry, and Quantum Chemical Calculations. *Chemical Reviews* **2017**, *117*, 3798–3881.

(6) Andrews, L.; Citra, A. Infrared Spectra and Density Functional Theory Calculations on Transition Metal Nitrosyls. Vibrational Frequencies of Unsaturated Transition Metal Nitrosyls. *Chemical Reviews* **2002**, *102*, 885–912.

(7) Blomberg, M. R. A.; Borowski, T.; Himo, F.; Liao, R.-Z.; Siegbahn, P. E. M. Quantum Chemical Studies of Mechanisms for Metalloenzymes. *Chemical Reviews* **2014**, *114*, 3601–3658.

(8) Siegbahn, P. E. M.; Blomberg, M. R. A. Quantum Chemical Studies of Proton-Coupled Electron Transfer in Metalloenzymes. *Chemical Reviews* **2010**, *110*, 7040–7061.

(9) Parr, R. G.; Yang, W., *Density-Functional Theory of Atoms and Molecules*; Oxford: 1989.

CHAPTER 4

EXAMPLES OF ELECTRON CORRELATION IN ORGANOMETALLIC CHEMISTRY

4.1 Vanadium oxo 2,6-bis[1,1-bis(2-pyridyl)ethyl]pyridine

4.1.1 Introduction

Recent experimental interest in the catalytic properties of organometallic complexes has generated significant questions about the nature of the reduction/oxidation (redox) event with respect to the metal center and its ligand field. It is well known that the redox properties of organometallic species can be dramatically altered via what are commonly known as non-innocent ligand effects.[1–7] In contrast the role of quantum entanglement, manifested through two-electron correlation, is not so well understood in the context of ligand non-innocence. Much work has shown that the nature of the redox event can be influenced by tuning the electronic structure of the ligand field.[8–12] As Wieghardt et al. suggested, however, there seems to be no a priori way of determining whether a redox event will be metal or ligand-centered.[13] Chang and coworkers have also suggested the importance of electron delocalization over ligand π orbitals in the apparent ligand-centered reduction of a cobalt species.[14] Furthermore, near degeneracies in the metal and ligand orbitals can provide for circumstances in which ligand-centered redox events become favored over metal centered events.[15,16] Both of these effects are clues suggesting that two-electron correlation effects may help tune ligand non-innocence, and may practically alter the character of a redox event.

We suggest, therefore, that predicting the ligand non-innocence of these species may re-

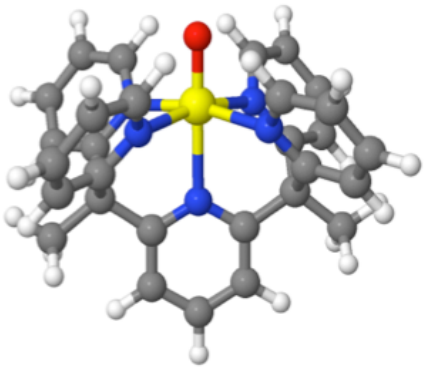

Figure 4.1: Structure of vanadium oxo 2,6-bis[1,1-bis(2-pyridyl)ethyl]pyridine. Vanadium is yellow, oxygen red, nitrogen blue, carbon grey, and hydrogen white.

quire a two-electron correlated description. Unfortunately, well-established electronic structure methods like density functional theory (DFT), as a single-reference method, or complete active space self-consistent field (CASSCF), as size limited, are systematically disadvantaged in dealing with these effects in species of this complexity. Therefore we present a study utilizing a two-electron correlated method that is generally applicable in the context of complicated redox chemistry of non-innocent ligands. We demonstrate that a large-scale, explicitly correlated method can be necessary to predict and characterize the ligand non-innocence in redox active organometallic complexes.

While vanadium oxo transition-metal complexes are important in catalytic, bioinorganic, and organometallic chemistries, the synthesis of a vanadium oxo complex with low-valent vanadium (III) has been elusive.[17–19] The recent reduction of vanadium (IV) oxo 2,6-bis[1,1-bis(2-pyridyl)ethyl]pyridine dication (Fig. 4.1) to a dark blue substance suggested the potential first synthesis of low-valent vanadium (III) in a vanadium oxo complex (monocation).[20] Despite its elusiveness, both ligand-field theory and conventional wave function calculations predict a metal-centered reduction of vanadium (IV) to vanadium (III) in the complex through the addition of an electron to the d_{xy} molecular orbital. Here we use large-scale calculations, based on the two-electron reduced density matrix (2-RDM),[21,22] to show that quantum entanglement redirects the electron transfer to the pyridine ligands. The calculations reveal that the reducing electron becomes entangled among the five pyridine ligands

with each ligand accepting a fraction (approximately one-fifth) of an electron. The results imply that the synthesis of a low-valent vanadium oxo complex remains elusive, but more importantly, reveal that the quantum entanglement, known for its central role in the Einstein-Podolsky-Rosen (EPR) paradox,[23,24] is responsible for altering the practical outcome of a chemical electron transfer process.

In a pure quantum state quantum entanglement occurs when a particle, such as an electron, has nonzero probability of being found in two or more domains where the domains may be characterized by distinct positions or momenta. Formally, a pure quantum state manifests entanglement between two or more domains if and only if its density matrix is not expressible as a product of the density matrices of each domain.[23,24] Furthermore, the correlation of N electrons is a special type of quantum entanglement in which the N-electron density matrix cannot be expressed as an anti-symmetrized product of one-electron density matrices.[21,22] Strong electron correlation is generally characterized as electron correlation that cannot be expressed as a small perturbation of an uncorrelated (non-entangled) state.

The variational 2-RDM theory is a powerful approach to describing strongly correlated, entangled electrons in molecular chemistry and condensed-matter physics.[25–34] Previous wave function calculations of the vanadium oxo complex did not correlate all of the electrons and orbitals of each ligand's π system due to computational limitations.[20] While recently developed wave function methods, like density matrix renormalization group, are potentially applicable, such methods have well-documented limitations from their required topological ordering of their orbitals, which has limited their applications to some transition-metal and bioinorganic complexes.[35,36] The present 2-RDM calculations, which are independent of the orbital order, use approximately a million variables in the 2-RDM to represent implicitly a wave function with sextillion (10^{21}) variables and thereby, correlate all of the π orbitals of the five pyridine ligands.[37] The larger 2-RDM-based calculations uncover a dramatically different quantum picture in which strong correlation and entanglement make ligand-centered reduction favorable over metal-center reduction. The redirection of electron transfer by

quantum entanglement as well as the computation of this redirection by 2-RDM methods have important implications for electron-transfer phenomena including catalysis in chemical and biological materials.

Two sets of advanced electronic structure calculations are analyzed to understand the quantum entanglement in the reduction of the vanadium (IV) oxo complex to the vanadium (III) oxo complex. In the first set, similar to prior calculations, 12 electrons and 10 orbitals on the vanadium and the oxygen are correlated. In general agreement with ligand-field theory and conventional chemical intuition, these calculations show a metal-centered reduction in which the electron adds to the vanadium. The electrons in the computed wave function (or 2-RDM) do not exhibit appreciable correlation or entanglement. A second set of much larger calculations, corresponding to 10^{21} quantum degrees of freedom, correlates 42 electrons and 40 orbitals on the vanadium, the oxygen, as well as all of electrons and orbitals associated with the π orbitals of pyridine ligands. From these calculations we find a ligand-centered reduction in which the reducing electron becomes entangled among the five pyridine ligands.

4.1.2 Results and Discussion

Comparison of the two starkly different results shows that quantum entanglement stabilizes the reduction of the pyridine ligands and thereby, redirects the electron transfer from the metal to the ligands. Hitherto, the second, larger calculation has not been attempted because it requires a conventional wave function with 10^{21} variables, which is a trillion times more variables than treatable by the fastest supercomputers. The present results were obtained by computing each molecule's 2-RDM directly without computation or storage of the many-electron wave function. The computed 2-RDM displays multiple signatures of the quantum entanglement including fractional occupations of the molecular orbitals and delocalization of the electron density to the pyridine ligands.[38]

Ligand-field theory predicts that in the reduction of the vanadium (IV) oxo complex to the vanadium (III) oxo complex an electron is added to the d_{xy} highest occupied molecular

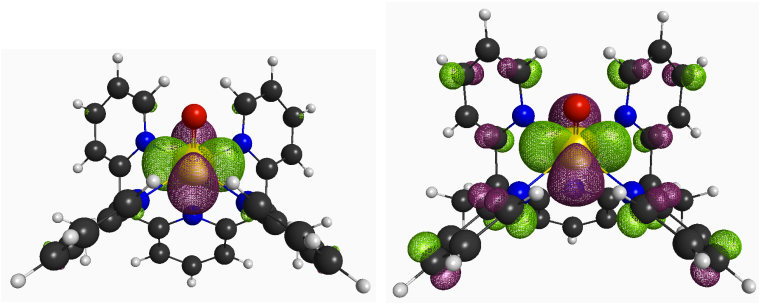

(a) (b)

Figure 4.2: Contour plots of electron density from the (HOMO) natural orbital of the (a) vanadium (IV) oxo and the (b) vanadium (III) oxo complexes are compared. The electron densities are computed at the [42,40] level of theory by the 2-RDM method. In (a) all of the electron density is located on the vanadium oxide moiety in agreement with the ligand-field picture. In (b), however, electron density is spread over not only vanadium oxide moiety but also the π space of the four equatorial pyridine ligands, reflecting the entanglement of the electron among the nearly energetically degenerate pyridine ligands. Generated with contour value 0.03, grid size 1, and 150 grid points. Vanadium is yellow, oxygen is red, nitrogens are blue, carbons are black, and hydrogens are white.

orbital (HOMO) on the vanadium atom of the complex.[39] Fig. 4.2 compares the contour plots of electron density from the HOMO natural orbital of the (a) vanadium (IV) oxo and the (b) vanadium (III) oxo complexes, respectively, computed by the [42,40] 2-RDM method where [42,40] denotes 42 electrons in 40 orbitals. In (a) all of the electron density is located on the vanadium oxide moiety in agreement with the ligand-field picture (Fig. 4.3). In (b), however, electron density is spread over not only the vanadium oxide moiety but also the π space of the four equatorial pyridine ligands. The contour-plot in (b) reveals a clear entanglement of the electron among the nearly energetically degenerate pyridine ligands.

Analysis of the computed 2-RDM of the vanadium (III) oxo complex in the larger [42,40] space reveals not only entanglement of the added (reducing) electron among the pyridine ligands but also strong correlation of the added electron and the remaining electrons in which the electronic wave function cannot be well represented by the perturbation of a mean-field wave function. An important manifestation of the strong electron correlation is appearance of partially occupied molecular orbitals, often called fractional orbital occupations. The fractional orbital occupations from the [42,40] 2-RDM calculations are contrasted schematically in Fig. 4.3 with the integer occupations from ligand field theory (LFT) and the [12,10] set.

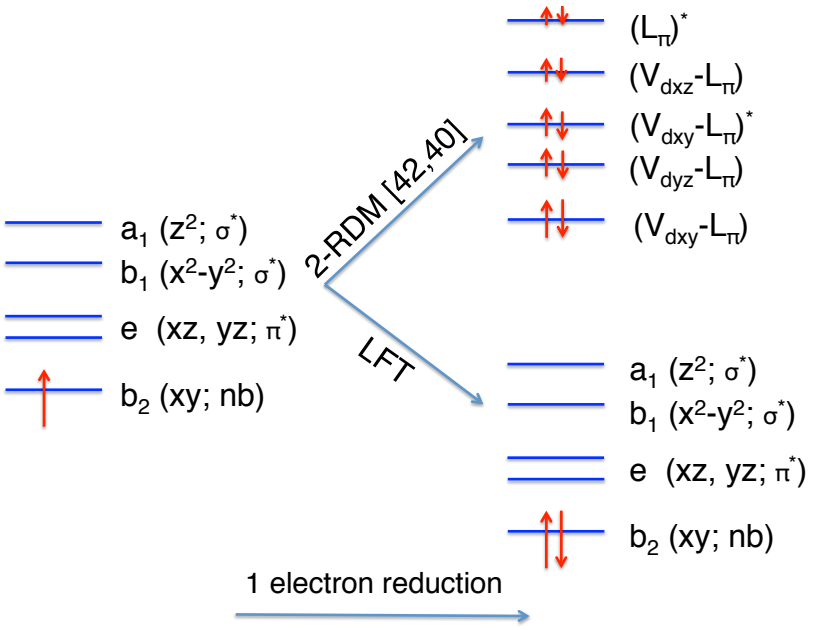

Figure 4.3: Ligand field theory (LFT) and 2-RDM theory predict different electronic pictures for the reduction of vanadium (IV) oxo (left) to vanadium (III) oxo (right). While the vanadium (IV) oxo complex's electronic structure can be well approximated by the schematic molecular orbital diagram from LFT (left), two different pictures of the vanadium (III) oxo product emerge from the [42,40] 2-RDM and LFT treatments (right). An LFT treatment results in an uncorrelated picture where electrons are localized at the vanadium (III) metal center, but a [42,40] 2-RDM treatment results in correlated electrons that are entangled throughout the ligand π manifold, where fractional occupation numbers are represented by arrows of different size.

Orbital Occupations						
	IV			III		
	LFT	[12,10]	[42,40]	LFT	[12,10]	[42,40]
HOMO - 1	2.000	1.913	1.881	2.000	1.974	1.876
HOMO	1.000	0.995	0.970	2.000	1.969	1.372
LUMO	0.000	0.087	0.147	0.000	0.031	0.258
LUMO + 1	0.000	0.056	0.106	0.000	0.026	0.221

Table 4.1: Orbital occupations indicate strong correlation and entanglement in the vanadium (III) complex with the [42,40] active space: a quantitative comparison of the occupations for the highest and lowest occupied molecular (natural) orbitals (HOMO and LUMO) as well as the next highest and next lowest orbitals (HOMO-1 and LUMO+1). While LFT is uncorrelated with HOMO and LUMO occupations of 2 and 0 and the [12,10] set is close to the LFT limit, the [42,40] set is strongly correlated with HOMO and LUMO occupations of 1.372 and 0.258, respectively.

The comparison of the [12,10] and [42,40] sets reveals starkly that the smaller orbital set masks important strong electron correlation and entanglement effects that only emerge in the larger [42,40] set when the π electrons (orbitals) of the pyridine ligands are allowed to correlate with each other and the electrons (orbitals) of the vanadium oxide moiety.

Table 4.1 provides a quantitative comparison of the occupations for the highest and lowest occupied molecular (natural) orbitals (HOMO and LUMO) as well as the next highest and next lowest orbitals. While LFT is uncorrelated with HOMO and LUMO occupations of 2 and 0, the [42,40] set is strongly correlated with HOMO and LUMO occupations of 1.372 and 0.258. Furthermore, the correlation responsible for the fractional occupations generates molecular orbitals that, in contrast to LFT and the [12,10] set, are substantially different from the traditional d orbitals of the vanadium metal (denoted by V in Fig. 4.3), displaying significant mixing with the ligand orbitals (denoted by L). Prior investigations only utilized the smaller orbital set and thereby masked the significant entanglement effects.

Charges from Mulliken population analysis are shown for different moieties of the vanadium (IV) and vanadium (III) oxo complexes in Table 4.2.[40] Mulliken populations reveal the approximate electron populations per atomic orbital. While Mulliken populations are most often computed from mean-field wave functions, in the present case they are computed from highly correlated calculations including [12,10] and [42,40] 2-RDM calculations. For

Mulliken Charges						
	[12,10] 2-RDM			[42,40] 2-RDM		
	IV	III	Δ	IV	III	Δ
1 Vanadium	1.724	1.587	-0.147	1.684	1.721	0.037
1 Oxygen	-0.493	-0.787	-0.305	-0.455	-0.479	-0.024
1 Pyridine$_{ax}$	0.22	0.134	-0.086	0.209	0.058	-0.151
4 Pyridine$_{eq}$	0.874	0.429	-0.444	0.872	0.046	-0.826
2 Ethyl	-0.336	-0.364	-0.028	-0.311	-0.346	-0.036

Table 4.2: Mulliken charges in the [12,10] and [42,40] sets provide two different pictures of reduction of the vanadium oxo complex. In the [12,10] 2-RDM calculation the decrease in the charge of the vanadium and oxygen atoms is substantial, which is in agreement with ligand-field theory's prediction of a metal-centered reduction. In contrast, the [42,40] 2-RDM calculation predicts a ligand-centered reduction in which the electron is primarily added to the pyridine ligands. The calculations were performed utilizing DQG N-representability conditions.

each complex charges are shown for the following moieties: (1) the vanadium atom, (2) the oxygen atom, (3) the four equatorial pyridine ligands, (4) the axial pyridine ligand, and (5) the four C_2H_3 groups connecting the equatorial pyridine ligands. Many types of population analysis are available, and all of them have their limitations; however, changes, Δ, in charge between the III and IV complexes, especially for collections of atoms such as the pyridine ligands, are less sensitive to the specific analysis. In this case we use the populations to summarize information contained in the computed 2-RDMs and reinforce other data such as the electron densities in Fig. 4.2.

In the [12,10] space, reduction of the vanadium oxo complex reduces the charges on the vanadium atom, the oxygen atom, and the pyridine ligands. The reduction of the vanadium and oxygen atoms is substantial, which is in reasonable agreement with ligand-field theory's prediction of a metal-centered reduction. In contrast, the [42,40] 2-RDM calculation shows no significant change in the net charge of the vanadium oxide moiety with the charge of the oxygen decreasing slightly and the charge of the vanadium actually increasing slightly. While prior investigations in restricted active spaces predicted a metal-centered reduction, the present large [42,40] calculations predict a ligand-centered reduction in which the electron is primarily added to the pyridine ligands. The reduction of the pyridine ligands is stabilized through strong electron correlation and entanglement effects that are

not included in either the ligand-field theory or the [12,10] electronic structure calculations. Because of the entanglement, each pyridine ligand only needs to accept one-fifth of the reducing electron.

The design of a spectroscopic experiment to probe the entangled electrons in the vanadium (III) oxo complex is an important open question. Vibrational spectroscopy, such as infrared spectroscopy, is not likely to provide a sufficiently clear signature of the entangled electrons. Even though the orbitals of the vanadium (III) oxo complex are fractionally occupied due to the entanglement, all of the electrons are spin paired because the vanadium (III) oxo complex has a singlet ground state. Consequently, electron paramagnetic resonance (EPR) spectroscopy cannot be employed to probe the molecular environment of the electrons. EPR has been applied to the doublet vanadium (IV) oxo complex,[20] but this complex is not predicted by the theory to show any entanglement. Furthermore, an EPR experiment on the triplet state of the vanadium (III) oxo complex would be a poor proxy for the ground singlet state because the triplet state is significantly higher than the singlet state. (DFT calculations show the triplet state to be 5-6 kcal/mol higher in energy than the singlet state[20] (8-9 kcal/mol in an STO-6G basis set) while parametric 2-RDM calculations[41] in a minimal (STO-6G) basis set show the triplet state to be 32.5 kcal/mol higher in energy than the singlet state. The singlet-triplet gap from the 2-RDM method is larger than the gap from DFT because the former method better captures the multi-reference correlation effects that stabilize the singlet state.

4.1.3 Conclusions

While the quantum entanglement of the Einstein-Podolsky-Rosen (EPR) paradox may seem esoteric, quantum entanglement has a significant role in real-world phenomena from superconductivity to photosynthesis.[42] Here we find that quantum entanglement redirects the electron transfer in the reduction of a transition metal vanadium oxo complex. While previous electronic structure calculations, restricted by computational limitations, supported

conventional chemical wisdom in predicting a metal-centered reduction, much larger calculations reveal a much richer interplay between chemistry and physics in which quantum entanglement stabilizes a ligand-centered addition. The electron added in the reduction becomes entangled among the pyridine ligands. The conventional chemical notion that pyridine is not a good oxidizing agent is overturned by quantum entanglement where in the entangled picture each pyridine ligand accepts only a fraction of the electron. The larger calculations, required to observe the quantum entanglement, were enabled by 2-RDM theory in which a two-electron quantity (2-RDM) with a million variables represents a wave function with sextillion (10^{21}) variables.[25,26] The use of quantum entanglement to alter the outcome of electron transfer in chemical processes has important chemical, physical, and biological applications to both the prediction and the control of electrons in catalysis and materials.

4.1.4 References

(1) Chiang, L.; Allan, L. E. N.; Alcantara, J.; Wang, M. C. P.; Storr, T.; Shaver, M. P. Tuning ligand electronics and peripheral substitution on cobalt salen complexes: structure and polymerisation activity. *Dalton Transactions* **2014**, *43*, 4295–4304.

(2) Kochem, A.; Thomas, F.; Jarjayes, O.; Gellon, G.; Philouze, C.; Weyhermüller, T.; Neese, F.; van Gastel, M. Structural and Spectroscopic Investigation of an Anilinosalen Cobalt Complex with Relevance to Hydrogen Production. *Inorganic Chemistry* **2013**, *52*, 14428–14438.

(3) Kochem, A.; Kanso, H.; Baptiste, B.; Arora, H.; Philouze, C.; Jarjayes, O.; Vezin, H.; Luneau, D.; Orio, M.; Thomas, F. Ligand Contributions to the Electronic Structures of the Oxidized Cobalt(II) salen Complexes. *Inorganic Chemistry* **2012**, *51*, 10557–10571.

(4) Allard, M. M.; Sonk, J. A.; Heeg, M. J.; McGarvey, B. R.; Schlegel, H. B.; Verani, C. N. Bioinspired Five-Coordinate Iron(III) Complexes for Stabilization of Phenoxyl Radicals. *Angewandte Chemie International Edition*, *51*, 3178–3182.

(5) Wile, B. M.; Trovitch, R. J.; Bart, S. C.; Tondreau, A. M.; Lobkovsky, E.; Milsmann, C.; Bill, E.; Wieghardt, K.; Chirik, P. J. Reduction Chemistry of Aryl- and Alkyl-Substituted Bis(imino)pyridine Iron Dihalide Compounds: Molecular and Electronic Structures of [$(PDI)_2Fe$] Derivatives. *Inorganic Chemistry* **2009**, *48*, 4190–4200.

(6) Bart, S. C.; Chłopek, K.; Bill, E.; Bouwkamp, M. W.; Lobkovsky, E.; Neese, F.; Wieghardt, K.; Chirik, P. J. Electronic Structure of Bis(imino)pyridine Iron Dichloride, Monochloride, and Neutral Ligand Complexes: A Combined Structural, Spectroscopic, and Computational Study. *Journal of the American Chemical Society* **2006**, *128*, 13901–13912.

(7) De Bruin, B.; Bill, E.; Bothe, E.; Weyhermüller, T.; Wieghardt, K. Molecular and Electronic Structures of Bis(pyridine-2,6-diimine)metal Complexes $[ML_2](PF6)_n$ (n = 0, 1, 2, 3; M = Mn, Fe, Co, Ni, Cu, Zn). *Inorganic Chemistry* **2000**, *39*, 2936–2947.

(8) Basu, D.; Allard, M. M.; Xavier, F. R.; Heeg, M. J.; Schlegel, H. B.; Verani, C. N. Modulation of electronic and redox properties in phenolate-rich cobalt(iii) complexes and their implications for catalytic proton reduction. *Dalton Transactions* **2015**, *44*, 3454–3466.

(9) Solis, B. H.; Yu, Y.; Hammes-Schiffer, S. Effects of Ligand Modification and Protonation on Metal Oxime Hydrogen Evolution Electrocatalysts. *Inorganic Chemistry* **2013**, *52*, 6994–6999.

(10) Ghosh, M.; Weyhermuller, T.; Wieghardt, K. Electronic structure of the members of the electron transfer series $[NiL]^z$ (z = 3+, 2+, 1+, 0) and [NiL(X)]n (X = Cl, CO, $P(OCH_3)_3$) species containing a tetradentate, redox-noninnocent, Schiff base

macrocyclic ligand L: an experimental and density functional theoretical study. *Dalton Transactions* **2010**, *39*, 1996–2007.

(11) Ray, K.; Petrenko, T.; Wieghardt, K.; Neese, F. Joint spectroscopic and theoretical investigations of transition metal complexes involving non-innocent ligands. *Dalton Transactions* **2007**, 1552–1566.

(12) Chun, H.; Verani, C. N.; Chaudhuri, P.; Bothe, E.; Bill, E.; Weyhermüller, T.; Wieghardt, K. Molecular and Electronic Structure of Octahedral o- Aminophenolato and o- Iminobenzosemiquinonato Complexes of V(V), Cr(III), Fe(III), and Co(III). Experimental Determination of Oxidation Levels of Ligands and Metal Ions. *Inorganic Chemistry* **2001**, *40*, 4157–4166.

(13) Sokolowski, A.; Adam, B.; Weyhermüller, T.; Kikuchi, A.; Hildenbrand, K.; Schnepf, R.; Hildebrandt, P.; Bill, E.; Wieghardt, K. Metal- versus Ligand-Centered Oxidations in PhenolatoVanadium and Cobalt Complexes: Characterization of Phenoxyl-Cobalt(III) Species. *Inorganic Chemistry* **1997**, *36*, 3702–3710.

(14) Nippe, M.; Khnayzer, R. S.; Panetier, J. A.; Zee, D. Z.; Olaiya, B. S.; Head-Gordon, M.; Chang, C. J.; Castellano, F. N.; Long, J. R. Catalytic proton reduction with transition metal complexes of the redox-active ligand bpy2PYMe. *Chemical Science* **2013**, *4*, 3934–3945.

(15) Messaoudi, S.; Robert, V.; Guihéry, N.; Maynau, D. Correlated ab Initio Study of the Excited State of the Iron-Coordinated-Mode Noninnocent Glyoxalbis(mercaptoanil) Ligand. *Inorganic Chemistry* **2006**, *45*, 3212–3216.

(16) Budzelaar, P. H. M.; de Bruin, B.; Gal, A. W.; Wieghardt, K.; van Lenthe, J. H. Metal-to-Ligand Electron Transfer in Diiminopyridine Complexes of MnZn. A Theoretical Study. *Inorganic Chemistry* **2001**, *40*, 4649–4655.

(17) Tsuji, J., *Transition Metal Reagents and Catalysis: Innovactions in Organic Synthesis*; Wiley: West Sussex, 2000.

(18) Hanson, S. K.; Baker, R. T.; Gordon, J. C.; Scott, B. L.; Sutton, A. D.; Thorn, D. L. Aerobic Oxidation of Pinacol by Vanadium(V) Dipicolinate Complexes: Evidence for Reduction to Vanadium(III). *Journal of the American Chemical Society* **2009**, *131*, 428–429.

(19) Son, S.; Toste, F. D. Non-oxidative vanadium-catalyzed C-O bond cleavage: application to degradation of lignin model compounds. *Angewandte Chemie International Edition English* **2010**, *49*, 3791.

(20) King, A. E.; Nippe, M.; Atanasov, M.; Chantarojsiri, T.; Wray, C. A.; Bill, E.; Neese, F.; Long, J. R.; Chang, C. J. A Well-Defined Terminal Vanadium(III) Oxo Complex. *Inorganic Chemistry* **2014**, *53*, 11388–11395.

(21) Coleman, A.; Yukalov, V., *Reduced Density Matrices: Coulson's Challenge*; Springer: New York, 2000.

(22) *Reduced-Density-Matrix Mechanics: With Application to Many-Electron Atoms and Molecules*; Mazziotti, D. A., Ed.; Advances in Chemical Physics, Vol. 134; John Wiley and Sons: Hoboken, New Jersey, 2007.

(23) Horodecki, R.; Horodecki, P.; Horodecki, M.; Horodecki, K. Quantum entanglement. *Review of Modern Physics* **2009**, *81*, 865–942.

(24) Huang, Z.; Wang, H.; Kais, S. Entanglement and electron correlation in quantum chemistry calculations. *Journal of Modern Optics* **2006**, *53*, 2543–2558.

(25) Mazziotti, D. A. Two-Electron Reduced Density Matrix as the Basic Variable in Many-Electron Quantum Chemistry and Physics. *Chemical Reviews* **2012**, *112*, 244–262.

(26) Mazziotti, D. A. Large-scale semidefinite programming for many-electron quantum mechanics. *Physical Review Letters* **2011**, *106*, 083001.

(27) Löwdin, P.-O. Quantum Theory of Many-Particle Systems. I. Physical Interpretations by Means of Density Matrices, Natural Spin-Orbitals, and Convergence Problems in the Method of Configurational Interaction. *Physical Review* **1955**, *97*, 1474–1489.

(28) Mayer, J. E. Electron Correlation. *Physical Review* **1955**, *100*, 1579–1586.

(29) Erdahl, R.; Jin, B. In *Many Electron Densities and Reduced Density Matrices*, Cioslowksi, J., Ed.; Kluwer: New York, 2004; Chapter 4.

(30) Hammond, J. R.; Mazziotti, D. A. Variational reduced-density-matrix calculation of the one-dimensional Hubbard model. *Physical Review A* **2006**, *73*, 062505.

(31) Rubin, N. C.; Mazziotti, D. A. Strong Electron Correlation in Materials from Pair-Interacting Model Hamiltonians. *Journal of Physical Chemistry C* **2015**, *119*, 14706–14713.

(32) Rothman, A. E.; Mazziotti, D. A. Variational reduced-density-matrix theory applied to the electronic structure of few-electron quantum dots. *Physical Review A* **2008**, *78*, 032510.

(33) Pelzer, K.; Greenman, L.; Gidofalvi, G.; Mazziotti, D. A. Strong Correlation in Acene Sheets from the Active-Space Variational Two-Electron Reduced Density Matrix Method: Effects of Symmetry and Size. *Journal of Physical Chemistry A* **2011**, *115*, 5632–5640.

(34) Greenman, L.; Mazziotti, D. A. Strong electron correlation in the decomposition reaction of dioxetanone with implications for firefly bioluminescence. *Journal of Chemical Physics* **2010**, *133*, 164110.

(35) Schollwöck, U. The density-matrix renormalization group. *Review of Modern Physics* **2005**, *77*, 259–315.

(36) McClean, J. R.; Aspuru-Guzik, A. Compact wavefunctions from compressed imaginary time evolution. *RSC Advances* **2015**, *5*, 102277–102283.

(37) Roos, B. O. In *Ab Initio Methods in Quantum Chemistry II*, Lawley, K., Ed.; Advances in Chemical Physics 69; Wiley: New York, 1987, pp 399–446.

(38) Piris, M.; Ugalde, J. M. Perspective on natural orbital functional theory. *International Journal of Quantum Chemistry*, *114*, 1169–1175.

(39) Ballhausen, C. J.; Gray, H. B. The Electronic Structure of the Vanadyl Ion. *Inorganic Chemistry* **1962**, *1*, 111–122.

(40) Mulliken, R. S. Electronic Population Analysis on LCAO–MO Molecular Wave Functions. I. *Journal of Chemical Physics* **1955**, *23*, 1833–1840.

(41) Mazziotti, D. A. Parametrization of the two-electron reduced density matrix for its direct calculation without the many-electron wave function. *Physical Review Letters* **2008**, *101*, 253002.

(42) Sarovar, M.; Ishizaki, A.; Fleming, G. R.; Whaley, K. B. Quantum entanglement in photosynthetic light-harvesting complexes. *Nature Physics* **2010**, *6*, 462–467.

4.2 Nickel Dithiolates

4.2.1 Introduction

Metal dithiolates are highly tunable,[1,2] and have a wide range of applications and properties including catalysis in water splitting and olefin transformations,[3–5] proton-coupled electron transfer,[6] non-linear optical responses,[7] and molecular conductivity and magnetization.[8–17] We examine the oxidation series of bis(ethylene-1,2-dithiolato) nickel, or $[\mathrm{Ni(edt)_2}]^{(-2,-1,0)}$ where edt is ethylene dithiolate ligand (Fig. 4.4), which is paradigmatic of other more substituted nickel dithiolate complexes.[18,19]

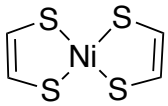

Figure 4.4: Skeletal structure of bis(ethylene-1,2-dithiolato)nickel, or $\mathrm{Ni(edt_2)}$

The electronic structure of metal dithiolates has been widely studied in the density functional theory (DFT) framework. DFT combined with X-ray absorption spectroscopy (XAS) data has shown that the ligands in these species act as the source or sink of electrons during the redox process, and the ligands are described as redox non-innocent.[20–26] Ligand non-innocence is not limited to metal dithiolates, however, and generally allows the metal ions to assume unexpected oxidation states.[27–30] In the case of nickel dithiolates the metal remains in a Ni(II) oxidation state throughout the oxidative series.[31] Along with a wide range of DFT studies on this class of molecules, several *ab initio* studies have largely focused on predicting the singlet-triplet gap of the neutral complex.[32–36] Finally, photoelectron[37–39] and femtosecond[40] spectroscopy have recently been used to study the ionization and ultrafast dynamics of these compounds.

We use two complementary 2-RDM methods to describe these compounds: the variational

two-electron reduced density matrix (2-RDM) and anti-Hermitian contracted Schrödinger equation (ACSE) methods (see Theory section for details).[41,42] The variational 2-RDM method scales polynomially in system size, unlike traditional *ab initio* wavefunction methods which scale exponentially, allowing variational 2-RDM to treat systems beyond the reach of wavefunction methods. Variational 2-RDM theory has been used to describe static correlation in a wide variety of applications including organometallic complexes, conducting polymers, quantum dots, organic molecules, and hydrogen chains.[43–52] Static (multi-reference) correlation arises when the electronic structure of a system cannot be describe by a single molecular-orbital diagram. Instead, two or more determinants must be included in the zeroth-order (reference) description of the correlation. These previous applications have shown the need for correlating large numbers of orbitals and electrons to capture entanglement beyond the limits of traditional wavefunction methods. In complete-active-space calculations the orbitals that are correlated are known as *active orbitals* while the orbitals that are not correlated are known as *inactive orbitals*. Here we compare two active spaces, one in which only the ligand π orbitals and electrons are correlated, and another in which both the ligand π and the five $3d$ orbitals of the nickel are correlated. While previous calculations on the nickel complex have only treated the π space as the active space, 2-RDM results from the of the vanadium oxo complex and manganese superoxide dismutase indicate that both the π and d orbitals must be correlated to achieve a reasonable description of the electron transfer.

ACSE has been applied to excited states in organic molecules, conjugated π systems, conical intersections, and photoexcitation reactions, where it has been shown to achieve a balanced description of static and dynamic correlation.[53–63] To compute the singlet-triplet energy gaps of the nickel complexes, we use the 2-RDM from the variational calculation as an initial guess for the solution of the ACSE. The ACSE correlates all of the orbitals in the molecule, capturing single-reference (dynamic) correlation from the inactive orbitals. Although the ACSE depends upon not only the 2-RDM but also the 3-RDM, we reconstruct

the 3-RDM from the 2-RDM by its cumulant expansion to approximate the solution to the ACSE.[64,65]

4.2.2 Theory and Computational Details

We use the variational 2-RDM method to generate a correlated 2-RDM for the active space. We seed the ACSE with this 2-RDM to further add the correlation from the inactive orbitals including their interaction with the active orbitals. Here we utilize the PYSCF package for the Hartree-Fock, integral generation, and orbital rotation steps for the variational 2-RDM method. We also use PYSCF for the wavefunction CASSCF and multi-reference second-order perturbation theory (MRPT2) calculations along with the DFT calculations and reported meta-Löwdin populations.[66,67]

We optimized all molecular structures enforcing D_{2h} point-group symmetry using the B3LYP[68,69] DFT functional with the GAMESS-US electronic structure package.[70,71] The z axis of the geometry is the normal of the square plane, and the x axis is oriented along the long axis of the molecule. We call the σ anti-bonding (B_{1g}) orbital the $d_{x^2-y^2}$ orbital by convention. We used a series of basis sets to study these molecules, cc-pVDZ, aug-cc-pVDZ, cc-pVTZ, and aug-cc-pVTZ, but because we did not find significant variation in the results, we report here the results from the cc-pVDZ basis set. The cc-pVDZ[72,73] basis set has been shown to be sufficient to model the fundamental, if not quantitative, chemistry of these complexes.[74]

We utilize three different active spaces in this study. The π space is a ten electron and eight orbital, or [10,8], active space for the neutral complex;[36] we denote the treatment of this space by the variational 2-RDM method as RDM(π). Including the eight $3d$ electrons in five $3d$ orbitals yields an [18,13] active space for the neutral complex, denoted by RDM(π & $3d$). We also study an [8,8] active space to study the singlet-triplet gap in the neutral complex, which is constructed from the molecular orbitals corresponding to the eight natural orbitals at the frontier of the [18,13] calculation. All core orbitals are frozen, i.e. they retain the

Hartree-Fock coefficients throughout the optimization. The molecular-orbital visualizations presented here were generated with GMolden.[75]

4.2.3 Results

Static Correlation and Nickel d Orbitals

The reason for choosing the π and nickel d orbitals derives from the XAS transition assignments for these complexes. In particular, the neutral complex exhibits transitions of metal to ligand σ donation through the B_{1g} orbital, and two transitions of B_{2g} and B_{3g} symmetry which are metal to ligand π back-donation. In the monoanion the σ donation transition is again present, along with a transition of a sulfur core electron to the ligand B_{2g} π transition.[22] While most other correlated studies have focused on the interplay of the π orbitals, we show here that explicitly correlating the metal d orbitals is important.

Table 4.3 shows the resulting differences between the two active spaces. In the π active

Table 4.3: Natural-Orbital Descriptions for $Ni(edt)_2$

	RDM(π)			RDM(π & $3d$)		
species	type	symmetry	occupation	type	symmetry	occupation
$[Ni(edt)_2]^{-2}$	π	A_u	1.999	d_{xz}	B_{2g}	1.939
	π	B_{1u}	1.922	π	B_{1u}	1.918
	π-d_{xz}	B_{2g}	1.920	π-d_{xz}	B_{2g}	1.911
	π-d_{yz}	B_{3g}	0.081	$d_{x^2-y^2}$	B_{1g}	0.133
$[Ni(edt)_2]^{-1}$	π-d_{xz}	B_{2g}	1.956	π	B_{1u}	1.862
	π	B_{1u}	1.867	d_{xz}	B_{2g}	1.411
	π-d_{xz}	B_{2g}	1.071	$d_{x^2-y^2}$	B_{1g}	0.986
	π-d_{yz}	B_{3g}	0.084	π-d_{xz}	B_{2g}	0.719
$[Ni(edt)_2]^{0}$	π	A_u	1.941	π	A_u	1.549
	π	B_{1u}	1.640	π	B_{1u}	1.343
	π-d_{xz}	B_{2g}	0.404	π-d_{xz}	B_{2g}	0.622
	π-d_{yz}	B_{3g}	0.064	$d_{x^2-y^2}$	B_{1g}	0.608

Natural-orbital occupation numbers, symmetries and dominant atomic orbital description from variational 2-RDM with DQGT conditions in both active spaces.

space the dianion and monoanion are single referenced, as indicated by the near integer

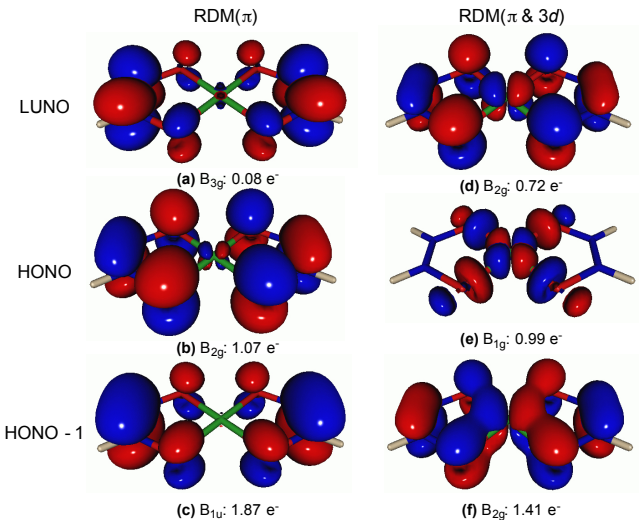

Figure 4.5: Visualized orbitals for the two active spaces in the monoanion with occupation numbers and symmetry below. The larger active space includes the singly occupied $3d_{x^2-y^2}$ orbital, along with two correlated B_{2g} orbitals, which are completely uncorrelated in the smaller active space.

occupation numbers of the active orbitals. On the other hand, the neutral species clearly exhibits multireference character based on the B_{1u}, B_{2g}, and B_{3g} orbital occupations. Inclusion of the d orbitals induces a significant change. Most interestingly we find that the monoanion exhibits multireference correlation with the inclusion of the d orbitals. There are two B_{2g} type orbitals which have fractional occupation, along with the lone electron in the B_{1g} orbital. While the small active space predicted a B_{2g} ground state, the large active space predicts a B_{1g} ground state. The fractional occupation numbers also yield insight into the biradicaloid nature of the neutral complex.[76]

The inclusion of the d orbitals does little to change the occupation spectrum of the dianion and neutral species. However, we observe that the last eight orbitals of the [18,13] active space, which includes the metal-based B_{1g} orbital, are critical to converging the active space to a solution similar to the [18,13] result. Although the resulting [8,8] active space is smaller than the π-only active space, it correlates several π and d orbitals, unlike the π only active space. In the discussion of the singlet-triplet gaps we will use the 2-RDM from the [8,8] active space to seed the solution of the ACSE.

Figure 4.5 visualizes the natural orbitals of the monoanion for the two active spaces.

Table 4.4: Ionization Potentials ($E_{\text{final}} - E_{\text{initial}}$) for $Ni(edt)_2$ (kcal/mol)

	ionization potential (kcal/mol)			
transition	Hartree-Fock	DFT	RDM(π)	RDM(π & 3d)
$[Ni(edt)_2]^{-2}$ to $[Ni(edt)_2]^{-1}$	-29.03	-51.36	-28.91	-41.67
$[Ni(edt)_2]^{-1}$ to $[Ni(edt)_2]^{0}$	70.71	56.95	45.17	58.91

The first oxidation is similar to the Hartree-Fock description when only correlating the π system. Including the 3d orbitals as well results in the second oxidation being very similar to the DFT/B3LYP result.

While the ligand π system plays a key role in the frontier orbitals in both cases, the natural-orbital occupation numbers are significantly different for the two active spaces. The inclusion of the $3d$ orbitals reveals the electron correlation in the B_{2g} orbitals (Fig. 4.5 **(d)** and **(f)**). The B_{2g} orbital in the π-only active space has slight mixing with the metal B_{2g} orbital (Fig. 4.5 **(b)**), but the important interactions between the metal and ligand B_{2g} orbitals is fully revealed only with the larger active space. Also, the monoanion is expected to be a Class III delocalized species, which means the species is not only delocalized, but is expected to have a non-integer valence occupation.[77,78] This fractional occupation scheme is only elucidated with the larger active space.

The different active spaces also predict differing degrees of static correlation and alters the predicted ionization potentials for this series. Table 4.4 shows the ionization potentials for Hartree-Fock, B3LYP, and the two active spaces studied here. We see that the small π-only active space replicates the Hartree-Fock result for the first ionization, which is expected because in this active space both the dianion and monoanion are not correlated. Since the small π space already predicts strong correlation in the neutral species, the second ionization is decreased relative to Hartree-Fock because of the correlation energy in the neutral species.

Because B3LYP treats the weakly correlated neutral molecule accurately but does not capture the static correlation of the monoanion, B3LYP overestimates the first ionization energy. In contrast, since both the monoanion and the neutral species in the larger active space are correlated, the second ionization energy from B3LYP is close to that from the 2-RDM method. The overestimation of the first correlation energy emphasize the challenge of

Table 4.5: $Ni(edt)_2$ Ligand Electron Count

species	ligand electron count[a]			
	Hartree-Fock	DFT	RDM(π)	RDM($\pi + 3d$)
$[Ni(edt)_2]^{-2}$	113.64	113.21	113.64	113.66
$[Ni(edt)_2]^{-1}$	112.59	112.26	112.59	112.76
$[Ni(edt)_2]^{0}$	111.57	111.25	111.56	111.57

[a] The electron count is given by meta-Löwdin population analysis and shows that vast majority of the oxidation occurs not in the nickel $3d$ orbitals, which indicates a Ni(II) species in all cases with a ligand-centered oxidation.

characterizing these species with single-reference methods that does not provide a balanced description of single- and multi-reference electron correlation.[74,79,80]

We can also examine the non-innocent nature of the ligand with a simple population analysis. Table 4.5 gives the meta-Löwdin populations for everything except nickel $3d$ orbitals. It is clear that for all methods studied here that the ligands are the source of the oxidized electron. In all cases there are about eight nickel $3d$ electrons implying a Ni(II) oxidation state. The differences associated with electron correlation do not affect the non-innocent ligand picture significantly.

Singlet-Triplet Gaps and Dynamic Correlation

It is known from experiment that both the dianion and neutral species have diamagnetic ground states, and calculations suggest a singlet diradical ground state for the neutral complex.[22] The degree of diradical character for metal dithiolates has been difficult to describe for a variety of reasons, and the results are strongly method dependent.[34,36,81] In contrast to the ligand non-innocence results discussed above, the singlet-triplet gap is sensitive to dynamic correlation not contained in the chosen active space.

We use MRPT2 (NEVPT2) and ACSE to describe the correlation beyond the active-space correlation energy. As described above, the iterative solution to the ACSE incorporates higher orders of perturbation theory than MRPT2.[42] For the neutral complex we checked

Table 4.6: $[Ni(edt)_2]^0$ Singlet-Triplet Gap (kcal/mol)

	E_{sing} - E_{trip} (kcal/mol)[a]			
	wavefunction methods		RDM methods	
Active-Space	CASSCF	NEVPT2	V2RDM	ACSE
$[8,8]$	-9.67	-12.99	-9.45	-18.14

[a] Negative gaps indicate singlet ground states.

for convergence in the active space, and determined that an [8,8] active space is large enough to observe the occupation spectrum in the [18,13] active space. We also checked for the importance of the second d-shell effect, but the natural-orbital occupation spectrum is basically invariant to the addition of the $4d$ orbitals.[82] With the second d-shell, an [18,18] active space is required, which is also the far limit of wavefunction CASSCF capabilities. We built the [8,8] active space using the Hartree-Fock orbitals corresponding to the last eight natural orbitals from the [18,13] calculation.

Table 4.6 compares the singlet-triplet gap for CASSCF, NEVPT2, variational 2-RDM and ACSE methods. Importantly, the variational 2-RDM and wavefunction CASSCF results are very similar, and the correlation included by ACSE or NEVPT2 widens the singlet-triplet gap considerably. We note that the singlet-triplet gap of the neutral species in the π and d active space is positive, implying a triplet ground state. Including dynamic correlation, however, yields a singlet ground state solution, and the ACSE result from the [8,8] active space is very similar to that of the larger active-space ACSE solution.

While the ACSE can match the accuracy of the larger active space with a pruned [8,8] active space including orbitals with the symmetries of critical π and d orbitals, the sufficiency of such a pruned active space may not be apparent until after a larger active-space calculation is performed. $Ni(edt_2)$ is the smallest of the nickel dithiolates, and expansion of the π system or including polymetallic systems will be far beyond the capabilities of wavefunction CASSCF, and therefore also beyond the reach of MRPT2 methods. Thus, the combination of variational 2-RDM and ACSE is a useful tool for describing these systems: checking for converging active spaces with variational 2-RDM, and capturing dynamic correlation with

ACSE regardless of the active-space size.

Balancing the static and dynamic correlation in these species is essential to achieve even a qualitatively correct picture of the singlet-triplet gap. Most studies have shown that the singlet is the ground state in the neutral complex, so the [18,13] CASSCF/RDM description fails in this respect. Some methods[32–34] have assigned a singlet ground state for species similar to this one with a singlet-triplet gap in the range of about 2000-9000 cm^{-1} or about 6-26 kcal/mol, which is consistent with the present results.

4.2.4 Conclusions

By comparing several correlation techniques including both wavefunction and RDM-based methods, we have elucidated various ways electron correlation plays a critical role in the electron transfer in nickel dithiolates. Entanglement of the electrons among the ligands leads to a ligand-centered oxidation, while correlation of the electrons between the metal d and ligand π orbitals contributes to nontrivial orbital filling in this oxidation series. Despite the transfer being almost entirely ligand-centered, calculations correlating the π and d orbitals reveal that the nickel $d_{x^2-y^2}$ orbital plays an important role in accurately characterizing the oxidation process. The monoanion is stabilized by a singly-occupied nickel $d_{x^2-y^2}$ orbital when it is included in the active space, in contrast to previous results that predict a π-type singly-occupied orbital, while neglecting the d orbitals in the active space.

The singlet-triplet gap of the neutral complex in the nickel dithiolate series offers another layer of complexity in the correlation picture. The complex, which is experimentally diamagnetic, should exhibit a singlet ground state. Calculations correlating the π-only or [8,8] active space predict singlet ground states, but including the full d orbital set leads to a triplet ground state. However, the experimentally correct ground state, we observe, can be recovered from the larger active spaces by including correlation of the inactive orbitals through the solution to the ACSE.

The metal dithiolates, in particular, provide a rich set of examples to prove ligand non-

innocence and electron correlation. In previous studies including the vanadium (III) oxo complex and the manganese superoxide dismutase mimic the connection between electron correlation and ligand non-innocence played an important role in the electron-transfer process. Large variational 2-RDM calculations beyond the degrees of freedom treatable by traditional wave functions were necessary to observe the stabilization of ligand-centered reduction from the entanglement of the reducing electron among the ligands (or ligand orbitals)..[43,45] For example, in the case of the vanadium oxo complex, active-space calculations using CASSCF, limited in size by memory constraints, do not capture the entanglement and hence, predict a metal-centered reduction.[45,83] In the present case we observe that electron correlation plays a critically important role in the fractional orbital occupations and singlet-triplet gap while contributing significantly but not exclusively to the ligand non-innocence. The present calculations, in conjunction with previous 2-RDM calculations, reveal that the effects of strong electron correlation must often be included for accurate prediction of orbital interactions, spin states, and non-innocent ligand effects.

The present 2-RDM study of nickel dithiolate can be expanded to more complex ligand and multi-metallic transition-metal complexes. While larger π spaces and additional metal d orbitals render wavefunction calculations like CASSCF and MRPT2 intractable, 2-RDM methods like the variational 2-RDM method and ACSE can treat such systems with a computational cost that grows polynomially with molecular system size. The present study of the nickel dithiolates provides an early step in using 2-RDM methods to study the relationship between electron correlation and chemical properties in the rich landscape of transition-metal based chemistries.

4.2.5 References

(1) Tsukada, S.; Kondo, M.; Sato, H.; Gunji, T. Fine electronic state tuning of cobaltadithiolene complexes by substituent groups on the benzene ring. *Polyhedron* **2016**, *117*, 265 –272.

(2) Bushnell, E. A. C.; Boyd, R. J. Identifying similarities and differences between analogous bisdithiolene and bisdiselenolene complexes: A computational study. *International Journal of Quantum Chemistry* **2016**, *116*, 369–376.

(3) Lv, H.; Ruberu, T. P. A.; Fleischauer, V. E.; Brennessel, W. W.; Neidig, M. L.; Eisenberg, R. Catalytic Light-Driven Generation of Hydrogen from Water by Iron Dithiolene Complexes. *Journal of the American Chemical Society* **2016**, *138*, 11654–11663.

(4) Raju, R. K.; Sredojevic, D. N.; Moncho, S.; Brothers, E. N. Nickel Bisdiselenolene as a Catalyst for Olefin Purification. *Inorganic Chemistry* **2016**, *55*, 10182–10191.

(5) Fan, Y.; Hall, M. B. How Electron Flow Controls the Thermochemistry of the Addition of Olefins to Nickel Dithiolenes: Predictions by Density Functional Theory. *Journal of the American Chemical Society* **2002**, *124*, 12076–12077.

(6) Kennedy, S. R.; Kozar, M. N.; Yennawar, H. P.; Lear, B. J. Steady-State Spectroscopic Analysis of Proton-Dependent Electron Transfer on Pyrazine-Appended Metal Dithiolenes [Ni(pdt)$_2$], [Pd(pdt)$_2$], and [Pt(pdt)$_2$] (pdt = 2,3-Pyrazinedithiol). *Inorganic Chemistry* **2016**, *55*, 8459–8467.

(7) Pilia, L.; Marinotto, D.; Pizzotti, M.; Tessore, F.; Robertson, N. High Second-Order NLO Response Exhibited by the First Example of Polymeric Film Incorporating a Diimine–Dithiolate Square-Planar Complex: The [Ni(o-phen)(bdt)]. *Journal of Physical Chemistry C* **2016**, *120*, 19286–19294.

(8) Branzea, D. G.; Pop, F.; Auban-Senzier, P.; Clérac, R.; Alemany, P.; Canadell, E.; Avarvari, N. Localization versus Delocalization in Chiral Single Component Conductors of Gold Bis(dithiolene) Complexes. *Journal of the American Chemical Society* **2016**, *138*, 6838–6851.

(9) Valade, L.; Faulmann, C. In *Conducting and Magnetic Organometallic Molecular Materials*,, M. F., Ouahab, L., Eds.; Topics in Organometallic Chemistry, Vol. 27; Springer-Verlag Berlin Heidelberg: 2009, p 141.

(10) Kubo, K.; Kato, R. In *Conducting and Magnetic Organometallic Molecular Materials*, Fourmigue, M., Ouahab, L., Eds.; Topics in Organometallic Chemistry, Vol. 27; Springer-Verlag Berlin Heidelberg: 2009, pp 35–53.

(11) Miyazaki, A.; Enoki, T. In *Conducting and Magnetic Organometallic Molecular Materials*, Fourmigue, M., Ouahab, L., Eds.; Topics in Organometallic Chemistry, Vol. 27; Springer-Verlag Berlin Heidelberg: 2009, pp 77–96.

(12) Kato, R. Conducting Metal Dithiolene Complexes: Structural and Electronic Properties. *Chemical Reviews* **2004**, *104*, 5319–5346.

(13) Stiefel, E. I., *Dithiolene Chemistry: Synthesis, Properties, and Applications*; Karlin, K. D., Ed.; Progress in Inorganic Chemistry, Vol. 52; John Wiley and Sons, Inc.: Hoboken, NJ, USA, 2003.

(14) Olk, R.-M.; Olk, B.; Dietzsch, W.; Kirmse, R.; Hoyer, E. The chemistry of 1,3-dithiole-2-thione-4,5-dithiolate (dmit). *Coordination Chemistry Reviews* **1992**, *117*, 99 –131.

(15) Coomber, A. T.; Beljonne, D.; Friend, R. H.; Bredas, J. L.; Charlton, A.; Robertson, N.; Underbill, A. E.; Kurmoo, M.; Day, P. Intermolecular interactions in the molecular ferromagnetic $NH_4Ni(mnt)_2{\cdot}H2O$. *Nature* **1996**, *380*, 144–146.

(16) Cassoux, P.; Valade, L.; Kobayashi, H.; Kobayashi, A.; Clark, R.; Underhill, A. Molecular metals and superconductors derived from metal complexes of 1,3-dithiol-2-thione-4,5-dithiolate (dmit). *Coordination Chemistry Reviews* **1991**, *110*, 115 –160.

(17) Mahadevan, C. 1,2-Dithiolene complexes of transition metals-structural systematics and physical properties. *Journal of Crystallographic and Spectroscopic Research* **1986**, *16*, 347–416.

(18) Bushnell, E. A. C.; Burns, T. D.; Boyd, R. J. The one-electron oxidation of a dithiolate molecule: The importance of chemical intuition. *Journal of Chemical Physics* **2014**, *140*, 18A519.

(19) Bushnell, E. A. C.; Burns, T. D.; Boyd, R. J. The one-electron reduction of dithiolate and diselenolate ligands. *Physical Chemistry Chemical Physics* **2014**, *16*, 10897–10902.

(20) Ray, K.; DeBeerGeorge, S.; Solomon, E.; Wieghardt, K.; Neese, F. Description of the Ground-State Covalencies of the Bis(dithiolato) Transition-Metal Complexes from X-ray Absorption Spectroscopy and Time-Dependent Density-Functional Calculations. *Chemistry – A European Journal* **2007**, *13*, 2783–2797.

(21) Queen, M. S.; Towey, B. D.; Murray, K. A.; Veldkamp, B. S.; Byker, H. J.; Szilagyi, R. K. Electronic structure of [Ni(II)S_4] complexes from S K-edge X-ray absorption spectroscopy. *Coordination Chemistry Reviews* **2013**, *257*, 564 –578.

(22) Sproules, S.; Wieghardt, K. Dithiolene radicals: Sulfur K-edge X-ray absorption spectroscopy and Harry's intuition. *Coordination Chemistry Reviews* **2011**, *255*, 837 –860.

(23) Eisenberg, R.; Gray, H. B. Noninnocence in Metal Complexes: A Dithiolene Dawn. *Inorganic Chemistry* **2011**, *50*, 9741–9751.

(24) Lim, B. S.; Fomitchev, D. V.; Holm, R. H. Nickel Dithiolenes Revisited: Structures and Electron Distribution from Density Functional Theory for the Three-Member Electron-Transfer Series $[Ni(S_2C_2Me_2)_2]^{0,1-,2-}$. *Inorganic Chemistry* **2001**, *40*, 4257–4262.

(25) Herman, Z. S.; Kirchner, R. F.; Loew, G. H.; Mueller-Westerhoff, U. T.; Nazzal, A.; Zerner, M. C. Electronic spectra and structure of bis(ethylene-1,2-dithiolato)nickel and bis-(propene-3-thione-1-thiolato)nickel. *Inorganic Chemistry* **1982**, *21*, 46–56.

(26) Ray, K.; Begum, A.; Weyhermüller, T.; Piligkos, S.; van Slageren, J.; Neese, F.; Wieghardt, K. The Electronic Structure of the Isoelectronic, Square-Planar Complexes $[FeII(L)_2]^{2-}$ and $[CoIII(LBu)_2]^{-}$ (L_2^- and $(LBu)_2^-$ = Benzene-1,2-dithiolates): An Experimental and Density Functional Theoretical Study. *Journal of the American Chemical Society* **2005**, *127*, 4403–4415.

(27) Kaim, W. Electron Transfer Reactivity of Organometallic Compounds Involving Radical-Forming Noninnocent Ligands. *Proceedings of the National Academy of Sciences, India Section A: Physical Sciences* **2016**, *86*, 445–457.

(28) Lyaskovskyy, V.; de Bruin, B. Redox Non-Innocent Ligands: Versatile New Tools to Control Catalytic Reactions. *ACS Catalysis* **2012**, *2*, 270–279.

(29) Kaim, W. The Shrinking World of Innocent Ligands: Conventionaland Non-Conventional Redox-Active Ligands. *European Journal of Inorganic Chemistry* **2012**, *2012*, 343–348.

(30) Hoffmann, R.; Alvarez, S.; Mealli, C.; Falceto, A.; Cahill 3rd, T. J.; Zeng, T.; Manca, G. From Widely Accepted Concepts in Coordination Chemistry to Inverted Ligand Fields. *Chemical Reviews* **2016**, *116*, 8173–92.

(31) Stiefel, E. I.; Waters, J. H.; Billig, E.; Gray, H. B. The Myth of Nickel(III) and Nickel(IV) in Planar Complexes. *Journal of the American Chemical Society* **1965**, *87*, 3016–3017.

(32) Herebian, D.; Wieghardt, K. E.; Neese, F. Analysis and Interpretation of Metal-Radical Coupling in a Series of Square Planar Nickel Complexes: Correlated Ab Initio and Density Functional Investigation of $[Ni(LISQ)_2]$ (LISQ=3,5-di-tert-butyl-o-diiminobenzosemiquinonate(1-)). *Journal of the American Chemical Society* **2003**, *125*, 10997–11005.

(33) Ray, K.; Weyhermüller, T.; Neese, F.; Wieghardt, K. Electronic Structure of Square Planar Bis(benzene-1,2-dithiolato)metal Complexes [M(L)2]z (z = 2, 1, 0; M = Ni, Pd, Pt, Cu, Au): An Experimental, Density Functional, and Correlated ab Initio Study. *Inorganic Chemistry* **2005**, *44*, 5345–5360.

(34) Bachler, V.; Olbrich, G.; Neese, F.; Wieghardt, K. Theoretical Evidence for the Singlet Diradical Character of Square Planar Nickel Complexes Containing Two o- Semi quinonato Type Ligands. *Inorganic Chemistry* **2002**, *41*, 4179–4193.

(35) Petrenko, T.; Ray, K.; Wieghardt, K. E.; Neese, F. Vibrational Markers for the Open-Shell Character of Transition Metal Bis-dithiolenes: An Infrared, Resonance Raman, and Quantum Chemical Study. *Journal of the American Chemical Society* **2006**, *128*, 4422–4436.

(36) Serrano-Andrés, L.; Avramopoulos, A.; Li, J.; Labéguerie, P.; Bégué, D.; Kellö, V.; Papadopoulos, M. G. Linear and nonlinear optical properties of a series of Ni-dithiolene derivatives. *Journal of Chemical Physics* **2009**, *131*, 134312.

(37) Waters, T.; Woo, H.-K.; Wang, X.-B.; Wang, L.-S. Probing the Intrinsic Electronic Structure of the Bis(dithiolene) Anions $[M(mnt)_2]^{2-}$ and $[M(mnt)_2]^{1-}$ (M = Ni, Pd, Pt; mnt = 1,2-$S_2C_2(CN)_2$) in the Gas Phase by Photoelectron Spectroscopy. *Journal of the American Chemical Society* **2006**, *128*, 4282–4291.

(38) Waters, T.; Wang, X.-B.; Woo, H.-K.; Wang, L.-S. Photoelectron Spectroscopy of the Bis(dithiolene) Anions $[M(mnt)_2]^{n-}$ (M = Fe Zn; n = 1, 2): Changes in Electronic Structure with Variation of Metal Center and with Oxidation. *Inorganic Chemistry* **2006**, *45*, 5841–5851.

(39) Liu, X.; Hou, G.-L.; Wang, X.; Wang, X.-B. Negative Ion Photoelectron Spectroscopy Reveals Remarkable Noninnocence of Ligands in Nickel Bis(dithiolene) Complexes [Ni(dddt)2] and [Ni(edo)2]. *Journal of Physical Chemistry A* **2016**, *120*, 2854–2862.

(40) Plyusnin, V. F.; Pozdnyakov, I. P.; Grivin, V. P.; Solovyev, A. I.; Lemmetyinen, H.; Tkachenko, N. V.; Larionov, S. V. Femtosecond spectroscopy of the dithiolate Cu(ii) and Ni(ii) complexes. *Dalton Transactions* **2014**, *43*, 17766–17774.

(41) Mazziotti, D. A. Two-Electron Reduced Density Matrix as the Basic Variable in Many-Electron Quantum Chemistry and Physics. *Chemical Reviews* **2012**, *112*, 244–262.

(42) Mazziotti, D. A. In *Reduced-Density-Matrix Mechanics: With Application to Many-Electron Atoms and Molecules*, Mazziotti, D. A., Ed.; John Wiley & Sons, Inc.: 2007, pp 19–59.

(43) McIssac, A. R.; Mazziotti, D. A. Ligand non-innocence and strong correlation in manganese superoxide dismutase mimics. *Physical Chemistry Chemical Physics* **2017**, *19*, 4656.

(44) Valentine, A. J. S.; Talapin, D. V.; Mazziotti, D. A. Orbitals, Occupation Numbers, and Band Structure of Short One-Dimensional Cadmium Telluride Polymers. *Journal of Physical Chemistry A* **2017**, *121*, 3142–3147.

(45) Schlimgen, A. W.; Heaps, C. W.; Mazziotti, D. A. Entangled Electrons Foil Synthesis of Elusive Low-Valent Vanadium Oxo Complex. *Journal of Physical Chemistry Letters* **2016**, *7*, 627–631.

(46) Pelzer, K.; Greenman, L.; Gidofalvi, G.; Mazziotti, D. A. Strong Correlation in Acene Sheets from the Active-Space Variational Two-Electron Reduced Density Matrix Method: Effects of Symmetry and Size. *Journal of Physical Chemistry A* **2011**, *115*, 5632–5640.

(47) Greenman, L.; Mazziotti, D. A. Strong electron correlation in the decomposition reaction of dioxetanone with implications for firefly bioluminescence. *Journal of Chemical Physics* **2010**, *133*, 164110.

(48) Van Aggelen, H.; Verstichel, B.; Bultinck, P.; Van Neck, D.; Ayers, P. W.; Cooper, D. L. Chemical verification of variational second-order density matrix based potential energy surfaces for the N_2 isoelectronic series. *Journal of Chemical Physics* **2010**, *132*, 114112.

(49) Verstichel, B.; van Aggelen, H.; Van Neck, D.; Ayers, P. W.; Bultinck, P. Variational determination of the second-order density matrix for the isoelectronic series of beryllium, neon, and silicon. *Physical Review A* **2009**, *80*, 032508.

(50) Greenman, L.; Mazziotti, D. A. Highly multireferenced arynes studied with large active spaces using two-electron reduced density matrices. *Journal of Chemical Physics* **2009**, *130*, 184101.

(51) Rothman, A. E.; Mazziotti, D. A. Variational reduced-density-matrix theory applied to the electronic structure of few-electron quantum dots. *Physical Review A* **2008**, *78*, 032510.

(52) Gidofalvi, G.; Mazziotti, D. A. Application of variational reduced-density-matrix theory to organic molecules. *Journal of Chemical Physics* **2005**, *122*, 094107.

(53) Greenman, L.; Mazziotti, D. A. Balancing single- and multi-reference correlation in the chemiluminescent reaction of dioxetanone using the anti-Hermitian contracted Schrödinger equation. *Journal of Chemical Physics* **2011**, *134*, 174110.

(54) Foley 4th, J. J.; Rothman, A. E.; Mazziotti, D. A. Strongly correlated mechanisms of a photoexcited radical reaction from the anti-Hermitian contracted Schrödinger equation. *Journal of Chemical Physics* **2011**, *134*, 034111.

(55) Gidofalvi, G.; Mazziotti, D. A. Direct calculation of excited-state electronic energies and two-electron reduced density matrices from the anti-Hermitian contracted Schrödinger equation. *Physical Review A* **2009**, *80*, 022507.

(56) Snyder, J. W.; Mazziotti, D. A. Photoexcited tautomerization of vinyl alcohol to acetylaldehyde via a conical intersection from contracted Schrodinger theory. *Physical Chemistry Chemical Physics* **2012**, *14*, 1660–1667.

(57) Snyder, J. W.; Mazziotti, D. A. Conical Intersection of the Ground and First Excited States of Water: Energies and Reduced Density Matrices from the Anti-Hermitian Contracted Schrödinger Equation. *Journal of Physical Chemistry A* **2011**, *115*, 14120–14126.

(58) Snyder, J. W.; Mazziotti, D. A. Photoexcited conversion of gauche-1,3-butadiene to bicyclobutane via a conical intersection: Energies and reduced density matrices from the anti-Hermitian contracted Schrödinger equation. *Journal of Chemical Physics* **2011**, *135*, 024107.

(59) Snyder, J. W.; Rothman, A. E.; Foley, J. J.; Mazziotti, D. A. Conical intersections in triplet excited states of methylene from the anti-Hermitian contracted Schrödinger equation. *Journal of Chemical Physics* **2010**, *132*, 154109.

(60) Greenman, L.; Mazziotti, D. A. Energy Barriers of Vinylidene Carbene Reactions from the Anti-Hermitian Contracted Schrödinger Equation. *Journal of Physical Chemistry A* **2010**, *114*, 583–588.

(61) Rothman, A. E.; Mazziotti, D. A. Nonequilibrium, steady-state electron transport with N-representable density matrices from the anti-Hermitian contracted Schrödinger equation. *Journal of Chemical Physics* **2010**, *132*, 104112.

(62) Foley, J. J.; Rothman, A. E.; Mazziotti, D. A. Activation energies of sigmatropic shifts in propene and acetone enolate from the anti-Hermitian contracted Schrödinger equation. *Journal of Chemical Physics* **2009**, *130*, 184112.

(63) Mazziotti, D. A. Determining the Energy Gap between the Cis and Trans Isomers of HO_3^- Using Geometry Optimization within the Anti-Hermitian Contracted Schrödinger and Coupled Cluster Methods. *Journal of Physical Chemistry A* **2007**, *111*, 12635–12640.

(64) Mazziotti, D. A. Contracted Schrödinger equation: Determining quantum energies and two-particle density matrices without wave functions. *Physical Review A* **1998**, *57*, 4219–4234.

(65) Mazziotti, D. A., *Reduced-Density-Matrix Mechanics: With Application to Many-Electron Atoms and Molecules*; Mazziotti, D. A., Ed.; Advances in Chemical Physics, Vol. 134; John Wiley and Sons: Hoboken, New Jersey, 2007; Chapter 8, p 165.

(66) Sun, Q.; Berkelbach, T. C.; Blunt, N. S.; Booth, G. H.; Guo, S.; Li, Z.; Liu, J.; McClain, J.; R.Sayfutyarova, E.; Sharma, S.; Wouters, S.; Chan, G. K.-L. The Python-based Simulations of Chemistry Framework (PySCF). *arXiv* **2017**, *arXiv:1701.08223*.

(67) Sun, Q.; Chan, G. K.-L. Exact and optimal quantum mechanics/molecular mechanics boundaries. *Journal of Chemical Theory and Computation* **2014**, *10*, 3784–3790.

(68) Becke, A. D. Density-functional thermochemistry. III. The role of exact exchange. *Journal of Chemical Physics* **1993**, *98*, 5648–5652.

(69) Lee, C.; Yang, W.; Parr, R. G. Development of the Colle-Salvetti Correlation-Energy Formula into a Functional of the Electron Density. *Physical Review B* **1988**, *37*, 785–789.

(70) Gordon, M.; Schmidt, M. In *Theory and Applications of Computational Chemistry: the first forty years*, Dykstra, C., Frenking, G., Kim, K., Scuseria, G., Eds.; Elsevier: Amsterdam, 2005, pp 1167–1189.

(71) Schmidt, M.; Baldridge, K.; Boatz, J.; Elbert, S.; Gordon, M.; Jensen, J.; Koseki, S.; Matsunaga, N.; Nguyen, K.; Su, S.; Windus, T.; Dupuis, M.; Montgomery, J. General Atomic and Molecular Electronic Structure System. *Journal of Computation Chemistry* **1993**, *14*, 1347–1363.

(72) Dunning, T. H. Gaussian basis sets for use in correlated molecular calculations. I. The atoms boron through neon and hydrogen. *Journal of Chemical Physics* **1989**, *90*, 1007–1023.

(73) Schuchardt, K. L.; Didier, B. T.; Elsethagen, T.; Sun, L.; Gurumoorthi, V.; Chase, J.; Li, J.; Windus, T. L. Basis Set Exchange: A Community Database for Computational Sciences. *Journal of Chemical Information and Modeling* **2007**, *47*, 1045–1052.

(74) Dang, L.; Yang, X.; Zhou, J.; Brothers, E. N.; Hall, M. B. Computational Studies on Ethylene Addition to Nickel Bis(dithiolene). *Journal of Physical Chemistry A* **2012**, *116*, 476–482.

(75) G.Schaftenaar; Noordik, J. Molden: a pre- and post-processing program for molecular and electronic structures. *Journal of Computer-Aided Molecular Design* **2000**, *14*, 123–134.

(76) Doehnert, D.; Koutecky, J. Occupation numbers of natural orbitals as a criterion for biradical character. Different kinds of biradicals. *Journal of the American Chemical Society* **1980**, *102*, 1789–1796.

(77) Day, P.; Hush, N. S.; Clark, R. J. Mixed valence: origins and developments. *Philosophical Transactions of the Royal Society of London A: Mathematical, Physical and Engineering Sciences* **2008**, *366*, 5–14.

(78) Demadis, K. D.; Hartshorn, C. M.; Meyer, T. J. The Localized-to-Delocalized Transition in Mixed-Valence Chemistry. *Chemical Reviews* **2001**, *101*, 2655–2686.

(79) Dang, L.; Ni, S. F.; Hall, M. B.; Brothers, E. N. Uptake of One and Two Molecules of 1,3-Butadiene by Platinum Bis(dithiolene): A Theoretical Study. *Inorganic Chemistry* **2014**, *53*, 9692–9702.

(80) Bushnell, E. A. C.; Boyd, R. J. Assessment of Several DFT Functionals in Calculation of the Reduction Potentials for Ni–, Pd–, and Pt–Bis-ethylene-1,2-dithiolene and -Diselenolene Complexes. *Journal of Physical Chemistry A* **2015**, *119*, 911–918.

(81) Illas, F.; Moreira, I. P. R.; de Graaf, C.; Barone, V. Magnetic coupling in biradicals, binuclear complexes and wide-gap insulators: a survey of ab initio wave function and density functional theory approaches. *Theoretical Chemistry Accounts* **2000**, *104*, 265–272.

(82) Dunning, T. H.; Botch, B. H.; Harrison, J. F. On the Orbital Description of the 4s3dn+1 States of the Transition Metal Atoms. *Journal of Chemical Physics* **1980**, *72*, 3419–3420.

(83) King, A. E.; Nippe, M.; Atanasov, M.; Chantarojsiri, T.; Wray, C. A.; Bill, E.; Neese, F.; Long, J. R.; Chang, C. J. A Well-Defined Terminal Vanadium(III) Oxo Complex. *Inorganic Chemistry* **2014**, *53*, 11388–11395.

4.3 Geometry Optimization of CrF_6 and Nickel Dithiolate Revisited

4.3.1 Introduction

Analytical gradient evaluation is an important tool for accurately and efficiently describing properties and geometries for electronic structure theory. Formulations of the analytical nuclear gradients have been described for a wide range of wavefunction methods. The first order gradient for Hartree-Fock is known as well as several higher order derivatives, and analytical gradients for many explicitly correlated methods have been described. Gradients for configuration interaction (CI) as well as several active space variants have been implemented,[1–7] along with analytical gradients of several multireference perturbation theory (MRPT) methods.[8–10] The coupled-cluster (CC) analytical gradients are known for CCSD, CCSD(T), and more recently described for CCSDT.[11–15] First and second order derivatives are known for natural orbital function theory (NOFT),[16,17] as well as for density-matrix renormalization group (DMRG).[18,19] Calculation of the CI gradient using a variationally optimized two-electron reduced density matrix (2-RDM) has also been recently implemented.[20]

The analytical gradient for the molecular electronic Hamiltonian is generally non-trivial to calculate because the basis set of atomic orbitals is typically centered on the nuclei, which results in complicated dependence on the overlap integral derivatives. The atomic orbital basis is in general not variationally optimized for the wavefunction, so the gradient does not take the simple form of the Hellmann-Feynman theorem.[21] Here we describe a transformation of the atomic orbital basis which allows for the variational optimization of all parameters that yields a gradient expression similar to the Hellmann-Feynman theorem. Direct minimization of the energy with respect to the transformed 2-RDM can be achieved using a semi-definite program (SDP) subject to N-representability constraints.[22–24] Analytical gradients of the full two-electron Hamiltonian can be used to study the geometry dependence of species when two-electron correlation is explicitly accounted for.

Electronic structure methods that accurately capture electron correlation are useful for describing molecules which cannot be described by a single-reference, or one-electron picture. These molecules must be described by multireference methods, which explicitly calculate the two-electron correlation energy that is neglected in a mean-field or Hartree-Fock picture. Traditional methods which explicitly calculate the electronic wavefunction scale exponentially in system size, which considerably limits the complexity of molecules those methods can treat. This unfavorable scaling can be avoided by recognizing that the electronic energy is an exact linear functional of the two-electron reduced density matrix (2-RDM). Here we utilize a polynomially scaling algorithm to generate the 2-RDM directly, instead of from the contraction of a wavefunction. This allows us to treat correlated systems far beyond the reach of traditional wavefunction methods. Here we present two examples of geometry optimizations using the analytical gradients of the molecular Hamiltonian. First we describe the CrF_6 molecule using a nearly full-valence active space, and predict the preferred conformation and bond lengths with good accuracy. We also describe the geometry dependence of correlation in a square-planar strongly correlated nickel complex.

Computational Details

All active space calculations were performed with the pyscf package using an integrated V2RDM module for the RDM-CASSCF calculations.[25] CCSD(T), Hartree-Fock, and DFT calculations were performed with GAMESS-US.[26,27] All DFT calculations were performed with the B3LYP functional.[28,29] Testing of other functionals (PBE0 and ωb97x-D) yielded similar results to B3LYP. The geometry optimization procedure for RDM-CASSCF is implemented in pyscf using the standard python package scipy to perform the BFGS optimization. The CASSCF geometry optimizations utilized no symmetry and is not a constrained optimization, while the CCSD(T), CCSD, Hartree-Fock, and DFT calculations are symmetry constrained optimizations for the CrF_6 results.

For the CrF_6 RDM-CASSCF calculations, we selected the initial guess orbitals from a

Hartree-Fock calculation. We include all fluorine $2p_z$ orbitals, the chromium $3d$ orbitals as well as the chromium $3p$ orbitals. This active space is 42 electrons in 26 spatial orbitals, or [42,26]. We present results from two basis sets: cc-pvdz, and cc-pvtz. Similar results were obtained in the aug-cc-pvdz basis.

We also present results from the nickel dithiolate compound, (ethylene-1,2-dithiolato)nickel, or $Ni(edt)_2$ (Fig 4.7). We expand upon recently published results to examine the geometry dependence of the electronic structures of the doublet monoanion and singlet neutral complex. We use an active space of all of the π and d orbitals ([19,13] for the monoanionic complex) and compute the optimal geometry using the V2RDM method as well as wavefunction generated RDMs. These calculations are computed with the cc-pvdz basis, and we compute both symmetry constrained and unconstrained geometries. Previous calculations were performed using B3LYP optimized geometries.

4.3.2 Results

CrF_6

Chromium hexafluoride (CrF_6) can exist in both an octahedral (O_h) or trigonal prismatic (D_{3h}) geometric conformation (Fig. 4.6). The strong covalency of the Cr-F bond suggests that static correlation effects should be important for this compound.[30] While we expect static correlation to be important in describing the electronic structure, calculations with small active spaces and no dynamic correlation included suggest that the D_{3h} conformer is energetically favored over the octahedron. Using the analytical gradients for CASSCF with V2RDM with a large active space we confirm that the O_h conformation is favored.

CrF_6 has proven challenging to describe spectroscopically as well as theoretically.[31–33] Theoretical methods utilizing Hartree-Fock, small active space CASSCF, and single reference perturbation theory indicated that the D_{3h} structure was favored.[34] Couple-cluster (CC) and multireference second-order perturbation theory (MRPT2), and density functional theory

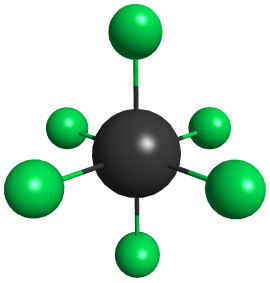

(a)

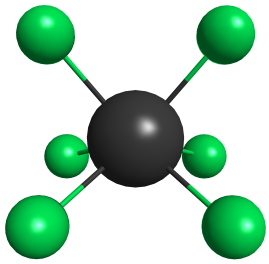

(b)

Figure 4.6: Structures for CrF_6 in octahedral, (a), and trigonal prismatic, (b), conformations

(DFT) on the other hand convincingly predict that the O_h structure is favored.[31,35,36] The success of CC and MRPT2 over Hartree-Fock and CASSCF suggests that the CrF_6 molecule has important energetic effects stemming from dynamic correlation, but active space studies utilizing MRPT2 also indicate that a multireference wavefunction is necessary for a quantitatively accurate MRPT2 result. CrF_6 provides a good example to test geometry optimization using a large active space to clarify the balancing of static and dynamic correlation in the energetic favorability of one conformer over the other.

The active space for CrF_6 is [42,26] which includes the five $3d$ and three $3p$ chromium orbitals, along with 18 fluorine $2p$ orbitals. MRPT2 studies with different active spaces showed that correlating the Cr $3p$ and F $2p$ orbitals significantly lowers the predicted barrier. Smaller active spaces with MRPT2 suggest that the O_h conformation is significantly more stable than the D_{3h} conformation relative to CCSD(T) results. A full [42,26] calculation was not possible with the RASPT2 method,[36] although a smaller calculation excluding the chromium $3p$ orbitals suggests that all fluorine $2p$ orbitals are essential in the active space.

Table 4.7: Differences in bond lengths and energies for various methods for two different conformations of CrF_6. The V2RDM result consistently predicts a longer bond than CCSD(T), and predicts a slightly smaller energy difference.

Basis	Method	ΔE (kcal/mol)[a]	r_{O_h} (Å)	$r_{D_{3h}}$ (Å)
cc-pvdz	V2RDM [42,26]	9.6	1.77	1.78
	CCSD(T)	11.9	1.74	1.75
	CCSD	-4.0	1.72	1.74
cc-pvtz	V2RDM [42,26]	10.5	1.74	1.75
	CCSD(T)	12.4	1.72	1.73
	CCSD	2.1	1.70	1.71
ANO-rcc	CASPT2[10,10] [b]	49.0	1.75	1.73
	RASPT2[42,26][b]	15.4-17.8	-	-

[a] $\Delta E = E_{D_{3h}} - E_{O_h}$

[b] These are the results of several RASPT2[42,26] single-point calculations[36] using the optimized geometries from the CASPT2[10,10] results.[37]

V2RDM is, on the other hand, capable of computing the 2-RDM of the active space including the $3p$ orbitals. We also computed the results from an active space excluding the chromium $3p$ orbitals, and while the trigonal prismatic species is higher in energy and the splitting is reasonable ($\sim$10 kcal/mol), the D_{2h} symmetric conformer is preferred over the O_h conformer. It is clear that all fluorine $2p$ and chromium $3p$ orbitals are required for an accurate active space picture.

The V2RDM results in Table 4.7 are very close to the CCSD(T) results. The overestimation of the bond lengths is likely due to N-representability error in the semidefinite programming optimization. N-representability error will overestimate the correlation energy in a system, and it will also tend to overestimate bond lengths by over-delocalizing the electron density. The failure of CCSD implies that the perturbative triples from the CCSD(T) method are essential for a correct description of the correlation. The V2RDM results correctly predict the relative energy from purely configuration interaction picture with no perturbative correction.

Table 4.8 shows the natural orbital occupation numbers from the V2RDM and CCSD calculations. Both the octahedral and trigonal prismatic complexes are similarly correlated.

Table 4.8: Natural orbital occupations near the occupied-unoccupied gap for the active space RDM calculation and CCSD for the octahedral conformation of CrF_6. All RDM results are from the [42,26] active space.

	O_h				D_{3h}			
	cc-pvdz		cc-pvtz		cc-pvdz		cc-pvtz	
Index	RDM	CCSD	RDM	CCSD	RDM	CCSD	RDM	CCSD
34	1.92	1.96	1.93	1.96	1.94	1.96	1.95	1.96
35	1.91	1.96	1.93	1.96	1.88	1.95	1.91	1.95
36	1.91	1.96	1.93	1.96	1.87	1.93	1.89	1.94
37	1.91	1.96	1.93	1.96	1.87	1.93	1.89	1.94
38	1.91	1.95	1.92	1.96	1.86	1.93	1.88	1.94
39	1.91	1.95	1.92	1.96	1.86	1.93	1.88	1.94
40	0.30	0.07	0.24	0.06	0.35	0.08	0.27	0.07
41	0.30	0.07	0.24	0.06	0.23	0.08	0.19	0.07
42	0.30	0.06	0.24	0.06	0.23	0.08	0.19	0.07
43	0.18	0.06	0.15	0.06	0.18	0.08	0.15	0.07
44	0.18	0.06	0.15	0.06	0.18	0.05	0.15	0.05

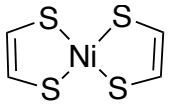

Figure 4.7: Skeletal structure of $Ni(edt)_2$.

The CCSD results, however, show significantly less multireference character compared to the V2RDM results, which is indicated by the lack of fractional occupation numbers near the occupied-unoccupied gap. The correlation that CCSD does not capture can be accounted for with CCSD(T), but is already accounted for with the V2RDM treatment.

Previous calculations involving the electronic structure of CrF_6 suggested that balancing static and dynamic correlation is essential for accurately comparing the two conformers. Our large active space calculations shows that both effects can be accounted for with a large enough active space. The relative energies and predicted bond lengths from the purely active space calculation are in good agreement with the CCSD(T) calculations, so the additional perturbative correction may be avoided with the large active space treatment.

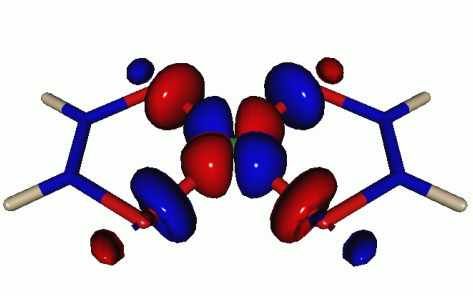

(a)

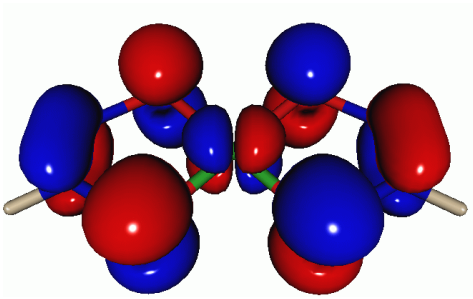

(b)

Figure 4.8: Representative natural orbitals for the Ni(edt)$_2$ complex. The B_{1g} σ-type orbital, (a), and the B_{2g} π-type orbital, (b), play an important role at the occupied-unoccupied gap in the monoanion Ni(edt)$_2$ complex.

Nickel Dithiolates

Recent RDM calculations showed that the doublet monoanionic species is a strongly correlated species with a previously unreported radical occupying the B_{1g} d_{xy}-type orbital, with significant occupation in the π-type B_{3g} orbital as well.[38] Furthermore, we showed that the singlet-triplet gap of the closed-shell species can be improved by additional calculations that include dynamic correlation. Here we examine both the neutral and monoanion and the effects of geometry on the electronic structure.

The monoanion case presents an interesting dependence on geometry. Previous single-point RDM calculations suggested that the metal-sulfer σ-antibonding orbital (B_{1g}) was singly occupied. This is in contrast to the DFT result which suggest that the π-type B_{2g} orbital was singly occupied. These orbitals are presented in Figure 4.8. The RDM results also indicated that the monoanion is multireferenced, with non-negligable occupation in the B_{2g} orbital. Optimizing the geometry with wavefunction CASSCF with the symmetry

Table 4.9: Selected bond lengths for the $[Ni(edt)_2]^{-1}$ optimized geometries for a [19,13] active space of the D_{2h} and C_1 wavefunctions as well as the C_1 V2RDM solution, and the B3LYP D_{3h} minimum.

Parameter	WF D_{2h}	WF C_1	RDM C_1	B3LYP D_{2h}
Ni-S1	2.4324	2.3058	2.3187	2.2167
Ni-S2	2.4324	2.3060	2.3189	2.2167
S1-C1	1.7242	1.7638	1.7466	1.7426
S2-C2	1.7242	1.7637	1.7466	1.7426
C1-C2	1.3720	1.3418	1.3544	1.3596

Table 4.10: Occupation numbers and atomic orbital description for $[Ni(edt)_2]^{-1}$ using a [19,13] active space including all π and nickel $3d$ orbitals.

	WF D_{2h}		WF C_1		RDM C_1	
Index	Occupation	Type	Occupation	Type	Occupation	Type
59	1.922	π	1.906	π	1.930	σ
60	1.379	π-d_{xz}	1.805	σ	1.527	π
61	1.047	d_{x^2-y2}	1.055	π-d_{xz}	1.028	π-d_{xz}
62	0.681	π-d_{xz}	0.238	d_{x^2-y2}	0.592	d_{x^2-y2}
63	0.077	π	0.085	π	0.047	π
64	0.069	π	0.083	π	0.009	π

constrained to the D_{2h} point group gives a similar result (Table 4.10). Intriguingly, when the symmetry constraint is relaxed, the complex slightly prefers (about 7mH) a non-symmetric solution which is closer to a C_{2v} conformation, and slightly shorter Ni-S bond lengths. Both the C_1 and D_{2h} solutions, however, predict slightly longer bond lengths than the B3LYP optimized geometry. While there is a stationary point on the C_1 B3LYP surface it is favored over the D_{2h} solution by only about 10^{-6} a.u.; we compare several geometries in Table 4.9.

Most significantly, the occupations of the B_{1g} and B_{2g} orbitals switch relative the D_{2h} solution, and the π-type orbital is predicted to be singly occupied (Table 4.10). Importantly, the degree of multireference correlation is similar for both the symmetric and non-symmetric solutions, which is indicated by the occupation spectrum.

Finally, we note that in our previous study of nickel dithiolates, the singlet-triplet gap of the neutral complex at the B3LYP optimized geometry with an active space of π and d orbitals was qualitatively incorrect. This active space predicting a triplet ground state. This was corrected either with the inclusion of dynamic correlation, or utilizing a smaller active

space. Optimizing the geometry using this active space resulted in a qualitatively correct singlet-triplet gap of about 4.3 kcal/mol, which is consistent with previously published results using several different methods.

In spite of several decades of probing with DFT and *ab initio* methods, it seems clear that the electronic structure of nickel dithiolates is not completely understood from an electron correlation perspective. These complexes are likely strongly influenced by multireference correlation, and that a careful treatment of correlation is important for finding energy minima on the potential energy surface. While in the case of the monoanion described above, the differences in geometric parameters between the DFT and RDM minima are not particularly striking, the stationary points provide significantly different pictures of the electronic structure. The neutral species has been studied as an example of a singlet diradical, and it the present results make clear that the relaxation of the geometry are important for predicting a qualitatively correct singlet-triplet gap.

4.3.3 Conclusions

Using a polynomially scaling correlated treatment of several transition metal complexes along with analytical gradients for the CASSCF wavefunction, we have demonstrated the importance of large active spaces in determining reasonable geometries for strongly correlated molecular systems. The CrF_6 results show that large active spaces are required to predict reasonable conformational energy differences without resorting to perturbative corrections. The case of the nickel dithiolates is intriguing since the electronic structure seems strongly influenced by slight changes in the geometry. The significant multireference character of these complexes, and their many analogues, will likely add another layer of complexity to the understanding of their ligand non-innocent character, as well as their interesting charge-transfer and other excited states.

The V2RDM method combined with the analytical gradients of the CASSCF ansatz provides a powerful tool to interrogate large active spaces and their geometric dependencies.

Molecules with extended π systems, multiple metal centers, and strongly covalent bonding all require large active spaces which are frequently out of reach for traditional wavefunction methods, but are tractable with V2RDM.

4.3.4 References

(1) Szalay, P. G.; Müller, T.; Gidofalvi, G.; Lischka, H.; Shepard, R. Multiconfiguration Self-Consistent Field and Multireference Configuration Interaction Methods and Applications. *Chemical Reviews* **2012**, *112*, 108–181.

(2) Pulay, P. In *Ab Initio Methods in Quantum Chemistry*, Lawley, K., Ed.; Wiley: 1987.

(3) Pulay, P. In *Modern Electronic Structure Theory Part 2*, Yarkony, D., Ed.; World Scientific: 1995.

(4) Taylor, P. R. Analytical MCSCF energy gradients: Treatment of symmetry and CASSCF applications to propadienone. *Journal of Computational Chemistry* **1984**, *5*, 589–597.

(5) Schlegel, H. B. In *Modern Electronic Structure Theory Part 2*, Yarkony, D., Ed.; World Scientific: 1995.

(6) Dupuis, M.; King, H. F. Molecular symmetry. II. Gradient of electronic energy with respect to nuclear coordinates. *Journal of Chemical Physics* **1978**, *68*, 3998–4004.

(7) Shepard, R. In *Modern Electronic Structure Theory Part 2*, Yarkony, D., Ed.; World Scientific: 1995.

(8) Nakano, H.; Hirao, K.; Gordon, M. S. Analytic energy gradients for multiconfigurational self-consistent field second-order quasidegenerate perturbation theory (MC-QDPT). *Journal of Chemical Physics* **1998**, *108*, 5660–5669.

(9) MacLeod, M. K.; Shiozaki, T. Communication: Automatic code generation enables nuclear gradient computations for fully internally contracted multireference theory. *Journal of Chemical Physics* **2015**, *142*, 051103.

(10) Vlaisavljevich, B.; Shiozaki, T. Nuclear Energy Gradients for Internally Contracted Complete Active Space Second-Order Perturbation Theory: Multistate Extensions. *Journal of Chemical Theory and Computation* **2016**, *12*, 3781–3787.

(11) Scheiner, A. C.; Scuseria, G. E.; Rice, J. E.; Lee, T. J.; III, H. F. S. Analytic evaluation of energy gradients for the single and double excitation coupled cluster (CCSD) wave function: Theory and application. *Journal of Chemical Physics* **1987**, *87*, 5361–5373.

(12) Lee, T. J.; Rendell, A. P. Analytic gradients for coupled-cluster energies that include noniterative connected triple excitations: Application to cis- and trans-HONO. *Journal of Chemical Physics* **1991**, *94*, 6229–6236.

(13) Gauss, J.; Stanton, J. F.; Bartlett, R. J. Coupled-cluster open-shell analytic gradients: Implementation of the direct product decomposition approach in energy gradient calculations. *Journal of Chemical Physics* **1991**, *95*, 2623–2638.

(14) Watts, J. D.; Gauss, J.; Bartlett, R. J. Open-shell analytical energy gradients for triple excitation many-body, coupled-cluster methods: MBPT(4), CCSD+T(CCSD), CCSD(T), and QCISD(T). *Chemical Physics Letters* **1992**, *200*, 1 –7.

(15) Gauss, J.; Stanton, J. F. Analytic gradients for the coupled-cluster singles, doubles, and triples (CCSDT) model. *Journal of Chemical Physics* **2002**, *116*, 1773–1782.

(16) Mitxelena, I.; Piris, M. Analytic gradients for natural orbital functional theory. *Journal of Chemical Physics* **2017**, *146*, 014102.

(17) Mitxelena, I.; Piris, M. Analytic second-order energy derivatives in natural orbital functional theory. *Journal of Mathematical Chemistry* **2018**.

(18) Dorando, J. J.; Hachmann, J.; Chan, G. K.-L. Analytic response theory for the density matrix renormalization group. *Journal of Chemical Physics* **2009**, *130*, 184111.

(19) Nakatani, N.; Guo, S. Density matrix renormalization group (DMRG) method as a common tool for large active-space CASSCF/CASPT2 calculations. *Journal of Chemical Physics* **2017**, *146*, 094102.

(20) Maradzike, E.; Gidofalvi, G.; Turney, J. M.; Schaefer, H. F.; DePrince, A. E. Analytic Energy Gradients for Variational Two-Electron Reduced-Density-Matrix-Driven Complete Active Space Self-Consistent Field Theory. *Journal of Chemical Theory and Computation* **2017**, *13*, 4113–4122.

(21) Bakken, V.; Helgaker, T.; Klopper, W.; Ruud, K. The calculation of molecular geometrical properties in the Hellmann—Feynman approximation. *Molecular Physics* **1999**, *96*, 653–671.

(22) Mazziotti, D. A. First-order semidefinite programming for the direct determination of two-electron reduced density matrices with application to many-electron atoms and molecules. *Journal of Chemical Physics* **2004**, *121*, 10957–66.

(23) Mazziotti, D. A. Large-scale semidefinite programming for many-electron quantum mechanics. *Physical Review Letters* **2011**, *106*, 083001.

(24) Gidofalvi, G.; Mazziotti, D. A. Spin and symmetry adaptation of the variational two-electron reduced-density-matrix method. *Physical Review A* **2005**, *72*, 052505.

(25) Sun, Q.; Berkelbach, T. C.; Blunt, N. S.; Booth, G. H.; Guo, S.; Li, Z.; Liu, J.; McClain, J.; R.Sayfutyarova, E.; Sharma, S.; Wouters, S.; Chan, G. K.-L. The Python-based Simulations of Chemistry Framework (PySCF). *arXiv* **2017**, *arXiv:1701.08223*.

(26) Gordon, M.; Schmidt, M. In *Theory and Applications of Computational Chemistry: the first forty years*, Dykstra, C., Frenking, G., Kim, K., Scuseria, G., Eds.; Elsevier: Amsterdam, 2005, pp 1167–1189.

(27) Schmidt, M.; Baldridge, K.; Boatz, J.; Elbert, S.; Gordon, M.; Jensen, J.; Koseki, S.; Matsunaga, N.; Nguyen, K.; Su, S.; Windus, T.; Dupuis, M.; Montgomery, J. General Atomic and Molecular Electronic Structure System. *Journal of Computation Chemistry* **1993**, *14*, 1347–1363.

(28) Lee, C.; Yang, W.; Parr, R. G. Development of the Colle-Salvetti Correlation-Energy Formula into a Functional of the Electron Density. *Physical Review B* **1988**, *37*, 785–789.

(29) Becke, A. D. Density-functional thermochemistry. III. The role of exact exchange. *Journal of Chemical Physics* **1993**, *98*, 5648–5652.

(30) Pierloot, K. In *Computational Organometallic Chemistry*, Cundari, T. R., Ed.; Marcel Dekker: 2001; Chapter 5, pp 123–158.

(31) Schlöder, T.; Brosi, F.; Freyh, B. J.; Vent-Schmidt, T.; Riedel, S. New Evidence in an Old Case: The Question of Chromium Hexafluoride Reinvestigated. *Inorganic Chemistry* **2014**, *53*, 5820–5829.

(32) Hope, E. G.; Levason, W.; Ogden, J. S. Is chromium hexafluoride octahedral? Experiment still suggests "yes!". *Inorganic Chemistry* **1991**, *30*, 4873–4874.

(33) Jacobs, J.; Mueller, H. S. P.; Willner, H.; Jacob, E.; Buerger, H. Vibrational and electronic spectra of molecular chromium tetrafluoride, CrF_4, and chromium pentafluoride, CrF_5. Comments on the existence of chromium hexafluoride, CrF_6. *Inorganic Chemistry* **1992**, *31*, 5357–5363.

(34) Marsden, C. J.; Wolynec, P. P. Is chromium hexafluoride octahedral? Theory suggests not! *Inorganic Chemistry* **1991**, *30*, 1681–1682.

(35) Vanquickenborne, L. G.; Vinckier, A. E.; Pierloot, K. A Density Functional Study of the Structure and Stability of CrF_4, CrF_5, and CrF_6. *Inorganic Chemistry* **1996**, *35*, 1305–1309.

(36) Vancoillie, S.; Zhao, H.; Tran, V. T.; Hendrickx, M. F. A.; Pierloot, K. Multiconfigurational Second-Order Perturbation Theory Restricted Active Space (RASPT2) Studies on Mononuclear First-Row Transition-Metal Systems. *Journal of Chemical Theory and Computation* **2011**, *7*, 3961–3977.

(37) Pierloot, K.; Roos, B. O. Is chromium hexafluoride octahedral? Theory confirms "yes!". *Inorganic Chemistry* **1992**, *31*, 5353–5354.

(38) Schlimgen, A. W.; Mazziotti, D. A. Static and Dynamic Electron Correlation in the Ligand Noninnocent Oxidation of Nickel Dithiolates. *Journal of Physical Chemistry A* **2017**, *121*, 9377–9384.